https://doi.org/10.5194/egusphere-2026-3557
Preprint. Discussion started: 26 June 2026

Separating Forced and Internal Contributions to Future Northern Hemisphere Storm Track Changes and Associated Precipitation Impacts

Karen E. Helliesen[1], Bosi Sheng[1,2,*], Massimo A. Bollasina[1]

[1]*School of Geosciences, University of Edinburgh, Edinburgh, UK*

[2]*Institute for Infrastructure and Environment, School of Engineering, University of Edinburgh, UK*

Correspondence: Bosi.Sheng@ed.ac.uk

Abstract

Storm tracks — the preferred pathways of extratropical cyclones in the midlatitudes — are projected to shift poleward, migrate upward in the atmosphere, and change in intensity under anthropogenic climate change. These changes have important consequences for weather and climate variability across the Northern Hemisphere (NH) midlatitudes. Here we investigate future changes in NH storm track strength and position, their driving physical mechanisms, and their impacts on precipitation, using large ensemble (LE) simulations from three CMIP6 models alongside ERA5 reanalysis data. Robust projections are developed under two scenarios (SSP2-4.5 and SSP5-8.5) for both boreal winter (DJF) and summer (JJA) at end-of-century (2070–2100) relative to the present day (1984–2014). The LE approach enables a rigorous characterisation of internal variability and the separation of the forced response from sampling noise. Key results include: (i) a poleward and upward shift of winter storm tracks, driven primarily by tropical upper-tropospheric warming that enhances upper-level baroclinicity, increasing precipitation poleward of ~45°N; (ii) a weakening of summer storm tracks associated with reduced static stability in the upper troposphere, leading to decreased precipitation across the midlatitudes; and (iii) substantial spread among ensemble members, particularly in DJF under SSP2-4.5, highlighting the prominent role of internal variability in shaping projected changes. The contribution of internal variability is reduced under SSP5-8.5 and during JJA, where the externally forced signal dominates. Inter-model differences, linked primarily to differing equilibrium climate sensitivities, emphasise the importance of multi-model LE frameworks for robust climate impact assessment.

1. Introduction

Storm tracks are regions of the midlatitudes through which extratropical cyclones (ETCs) preferentially travel, forming a central component of the global circulation by transporting heat, moisture, and momentum poleward (Chang and Fu, 2002). In the Northern Hemisphere (NH), the principal storm tracks are located over the North Atlantic and

https://doi.org/10.5194/egusphere-2026-3557
Preprint. Discussion started: 26 June 2026

North Pacific (Hoskins and Hodges, 2002). Regional weather and climate over Eurasia and North America are therefore strongly controlled by the strength and position of these features. ETCs account for a large fraction of total and extreme precipitation, as well as high surface wind speeds in these regions (Lehmann et al., 2014). Indeed, ETCs account for approximately 70–80% of all precipitation in the mid-latitude storm track regions (Hawcroft et al., 2012), underlining their fundamental role not only in extreme events but in the mean hydrological cycle of the midlatitudes. The socioeconomic consequences are substantial: flooding, infrastructure damage, and power disruption associated with ETC activity motivate the need to anticipate how storm tracks will respond to a changing climate (Laurila et al., 2021). ETC-associated precipitation is a primary driver of mid-latitude flooding events, with individual intense cyclones capable of producing rainfall totals sufficient to cause severe inundation within 24–48 hours (Hawcroft et al., 2018). Understanding how such events will change under warming is therefore directly relevant to flood risk management and adaptation planning. ETCs have also been shown to account for more than 80% of precipitation extremes in the NH midlatitudes when the contribution of associated fronts is included (Catto et al., 2011), underscoring their disproportionate role in shaping high-impact weather. Pfahl and Wernli (2012) further showed that ETCs are responsible for a large share of precipitation extremes globally, providing a robust quantitative basis for linking storm track changes to future shifts in extreme event frequency.

Storm tracks exhibit a pronounced annual cycle: they are strongest during boreal winter (DJF) and retain much of this intensity into spring, weaken substantially in summer (JJA), most markedly over the North Pacific, and re-intensify in autumn (Hoskins and Hodges, 2019). This seasonal contrast reflects the seasonal modulation of baroclinic instability and sets the baseline against which climate-change-induced shifts occur.

It is well established that global warming will alter the dynamics of storm tracks. ETCs develop from baroclinic instability driven by the meridional temperature gradient, which is directly affected by anthropogenic warming through two competing mechanisms operating at different levels of the troposphere. Near the surface, polar amplification, the tendency of the Arctic to warm faster than the tropics (Holland and Bitz, 2003; Lu and Cai, 2009), weakens the lower-tropospheric meridional temperature gradient at midlatitudes, reducing baroclinicity and weakening the storm tracks. In the mid-to-upper troposphere, however, enhanced tropical warming through moist-adiabatic adjustment strengthens the upper-level temperature gradient between the tropics and poles, increasing upper-level wind shear and baroclinicity and favouring a poleward shift and upward intensification of storm track activity (Held, 1993; Shaw et al., 2016). The net response of winter storm tracks therefore reflects the balance between these two opposing effects, making the projected magnitude and spatial pattern of change sensitive to the relative strength of these competing forcings (Coumou et al., 2015; Shaw et al., 2016). It should be noted that both polar amplification and the upper-level warming pattern will also reflect the combined effects of greenhouse gas increases and reductions in anthropogenic aerosol emissions, rather than GHG forcing alone. Aerosol reductions, particularly over Europe, North America, and East Asia where historical aerosol loading has been the largest, contribute substantially to projected regional warming patterns and have been shown to influence NH midlatitude circulation and storm track variability on both historical and future timescales (Undorf et al., 2018; Kang et al., 2024). The relative magnitudes of these two forcings, greenhouse gas increases and aerosol reductions, vary across future emission pathways, adding further complexity to the interpretation of scenario-dependent storm track changes.

https://doi.org/10.5194/egusphere-2026-3557
Preprint. Discussion started: 26 June 2026

Recent work using the Polar Amplification Model Intercomparison Project (PAMIP) further clarifies that Arctic sea-ice loss produces a regional "tug-of-war" in the North Atlantic, with sea-ice loss shifting the storm track equatorward and ocean warming shifting it poleward, whereas these two forcings reinforce each other in the North Pacific (Screen et al., 2025). Despite this regional complexity, there is broad consensus in the literature that NH storm tracks will shift poleward and upward in the atmosphere during boreal winter, and weaken during boreal summer (Yin, 2005; Chang et al., 2012; Shaw et al., 2016). The projected summer weakening, attributed to human influence with high confidence (Chemke and Coumou, 2024; Shaw et al., 2024), counteracts the thermodynamically driven increase in precipitation associated with higher atmospheric moisture content (Seneviratne et al., 2021). This competing influence, thermodynamic moistening acting to intensify precipitation versus dynamic storm track weakening suppressing ETC activity, is particularly important in summer and motivates the explicit decomposition of storm-track-driven versus total precipitation changes carried out in this study. Even under scenario uncertainty in the circulation response, Hawcroft et al. (2018) showed that ETC-associated extreme precipitation is robustly projected to increase over Europe and North America due to thermodynamic moisture loading alone, suggesting that the net precipitation response depends critically on the balance between these competing effects.

Observed trends are broadly consistent with these projections. Reanalysis-based analyses show that NH winter storm tracks strengthened during the second half of the twentieth century over both the Pacific and Atlantic (Geng and Sugi, 2001; Graham and Diaz, 2001; Chang and Fu, 2002), with more recent work by Karwat et al. (2022) confirming ETC intensification in ERA5 data for 1950–2021. Meridional wind variance increased by 10% or more in the winter Pacific and by a smaller amount in the Atlantic during the satellite era (Chang and Yau, 2016). In contrast, summer ETC activity declined by approximately 4% per decade from 1979 to 2014 (Chang et al., 2016), with Chemke and Coumou (2024) documenting a ~6% overall weakening between 1979 and 2020. Alongside these intensity trends, the total count of NH ETCs has declined since the mid-twentieth century (Priestley and Catto, 2022), highlighting a key difference between changes in the overall cyclone number and changes in the most intense events. The latter have shown evidence of strengthening (Hawcroft et al., 2018; Jucker et al., 2025), suggesting that future precipitation impacts will increasingly be concentrated in the high-intensity tail of the ETC distribution, the regime targeted by the composite analysis employed here. The ability of CMIP6 models to replicate this observed summertime weakening has been identified as a partial success relative to CMIP5, with the improvement linked in part to updated aerosol forcing (Simpson et al., 2025). The IPCC AR6 reports medium confidence that storm tracks have been shifting poleward since the 1980s, but low confidence in long-term trends in the intensity of the strongest ETCs due to large interannual and decadal variability (Seneviratne et al., 2021).

Despite this broad agreement, substantial uncertainty remains in projected storm track changes. CMIP6 models have improved the representation of storm tracks compared to earlier phases but still display persistent biases, particularly in the North Pacific (Harvey et al., 2020). Harvey et al. (2020) showed that while Atlantic and summer storm track biases have diminished substantially from CMIP3 to CMIP6, the winter North Pacific bias has persisted across all three CMIP phases, and noted that the larger CMIP6 climate responses relative to CMIP5 are consistent with the overall increase in equilibrium climate sensitivity (ECS) across the ensemble. Priestley and Catto (2022) found that the total number of NH cyclones decreases by ~5% by the end of the 21st century in CMIP6 under all

https://doi.org/10.5194/egusphere-2026-3557
Preprint. Discussion started: 26 June 2026

scenarios examined, but the area of extreme wind speeds in winter cyclones under the intermediate Shared Socioeconomic Pathway scenario (SSP2-4.5) increased by less than half the amount projected under the high-emission scenario (SSP5-8.5), illustrating that mitigation substantially reduces peak storm impacts. A recent preprint (Mercier et al., 2026) reinforces the view that despite weakening near-surface temperature gradients, intensifying atmospheric moisture content may drive stronger extreme North Atlantic cyclones, suggesting a shift toward moisture-driven rather than baroclinicity-driven dynamics for the tail of the ETC distribution. Importantly, internal climate variability can obscure the externally forced signal, especially under moderate emission scenarios and during winter, when ETC activity is strongest (Deser et al., 2020). Quantifying the relative contributions of external forcing and internal variability is therefore essential for producing reliable projections and informing risk assessment. Priestley et al. (2024) highlighted that internal variability can dominate short-to-medium-term uncertainty in European windstorm projections when only a single or small number of ensemble members are available, underscoring the value of large ensembles (LEs) for robustly separating the forced response from internal noise. For climate adaptation and risk management, this distinction is critical: a single realisation drawn from within the plausible range of internal variability may yield projections far above or far below the forced signal, potentially misguiding infrastructure investment or flood risk policy decisions (Deser et al., 2020; Mankin et al., 2020).

Previous multi-model studies of storm track change have predominantly used a single ensemble member per model to maximise structural diversity (Chang et al., 2022; Chemke and Coumou, 2024). While this maximises model variety, it limits the ability to characterise internal variability. The full range of plausible future outcomes within each model LE simulations, in which many members are initialised from slightly perturbed conditions, offer a complementary approach: with a smaller set of models but many realisations per model, they allow the forced response to be cleanly separated from internal variability (Deser et al., 2020; García-Martínez and Bollasina, 2021). The importance of this framework for storm tracks specifically was underscored by Hess and Chemke (2025), who used a LE spanning the last millennium to show that natural forcings alone intensified the North Atlantic summer storm track in the past centuries through high-latitude cooling, demonstrating that the internally chaotic nature of midlatitude storms necessitates LEs even for detecting multi-centennial forced signals. Similarly, Jucker et al. (2025) identified five hotspots of ETC-associated extreme precipitation in CMIP6 and documented future increases in the intensity of precipitating ETCs despite a declining cyclone frequency. Despite the broad agreement that NH storm tracks will shift poleward in winter and weaken in summer under anthropogenic warming, the relative roles of external forcing and internal variability remain poorly constrained.

This study uses LE CMIP6 simulations from three models — EC-Earth3, CanESM5, and MPI-ESM1.2-LR (hereafter MPI) — each providing 50 ensemble members (20 for CanESM5 future scenarios), to investigate projected changes in NH storm tracks and their precipitation impacts. We examine both DJF and JJA, two climate scenarios (SSP2-4.5 and SSP5-8.5), and the North Atlantic and North Pacific separately. Key contributions relative to existing literature are: (1) a rigorous quantification of internal variability in storm track projections using LE models; (2) an analysis of the season- and scenario-dependence of the forced-to-internal variability ratio; and (3) a linkage between projected storm track changes and precipitation impacts via percentile-based composite analysis over both basins and

https://doi.org/10.5194/egusphere-2026-3557
Preprint. Discussion started: 26 June 2026

their adjacent land areas, explicitly partitioning storm-track-driven from residual precipitation changes (extending the European analysis of Chang et al. (2022) to the full NH domain).

2 Data and Methods

2.1 Models and reanalysis

We use LE simulations from three CMIP6 Earth System Models: EC-Earth3 (Döscher et al., 2022), CanESM5 (Swart et al., 2019), and MPI (Olonscheck et al., 2023), all available through the Multi-Model Large Ensemble Archive (MMLEA; (Deser et al., 2020)). EC-Earth3 and MPI each provide 50 ensemble members; for CanESM5, 50 historical members are available but only 20 are available for future scenarios (SSP2-4.5 and SSP5-8.5), so we use the first 20 members for both historical and future periods (Table S1). The models span a wide range of ECS: 4.3 K for EC-Earth3 (Wyser et al., 2020), 5.6 K for CanESM5 (Virgin et al., 2021), and 2.8 K for MPI (Maher et al., 2019), making them a representative sample of CMIP6 model sensitivity. The three models span much of the CMIP6 ECS range, capturing both high and moderate climate sensitivity responses; this spread is exploited in the analysis to assess the role of model thermodynamic sensitivity in shaping projected storm track changes.

Atmospheric horizontal resolutions are approximately 0.7°×0.7° (EC-Earth3), 1.9°×1.9° (MPI), and 2.8°×2.8° (CanESM5). All three models have been shown to reproduce the large-scale atmospheric circulation and the historical storm track climatology with reasonable fidelity (Deser et al., 2020; Priestley et al., 2020), providing confidence in their use for projection analysis. Present-day simulations (1984–2014) are evaluated against ERA5 reanalysis data (Hersbach et al., 2020) at 0.25°×0.25° horizontal resolution. The end-of-century period is defined as 2070–2100 to maximise the contrast in radiative forcing between the two scenarios (Rivosecchi et al., 2024). All three models provide LE simulations under all four core ScenarioMIP scenarios (SSP1-2.6, SSP2-4.5, SSP3-7.0, and SSP5-8.5). We select SSP2-4.5 and SSP5-8.5 as they encompass the most policy-relevant range of outcomes: SSP2-4.5 is broadly consistent with current global emissions trajectories and therefore represents a plausible near-term future (~2.7°C warming above pre-industrial by 2100; (Hausfather and Peters, 2020)), while SSP5-8.5 represents the high-emissions upper bound (~5°C), maximising the contrast between a currently plausible pathway and a high-end sensitivity scenario that, while increasingly unlikely given current emissions trajectories, provides an upper bound on potential storm track changes and is widely retained in the literature for this purpose (Hausfather and Peters, 2020; Rivosecchi et al., 2024).

2.2 Storm track diagnostic

Storm track activity can be quantified through two complementary diagnostic frameworks. Lagrangian cyclone-tracking methods follow individual cyclone centres through their lifecycles, yielding information on frequency, intensity, and trajectory (Bell and Bosart, 1989; Murray and Simmonds, 1991; Hodges, 1999). Alternatively, Eulerian band-pass filtered variance statistics provide continuous spatial distributions of synoptic-scale transient eddy activity (Blackmon, 1976; Wallace et al., 1988; Chang et al., 2012). The latter approach, adopted here, has been shown to be highly correlated with both precipitation and wind impacts (Yau and Chang, 2020) and is particularly well-suited to large-ensemble analysis: ensemble-mean variance fields can be computed efficiently across

https://doi.org/10.5194/egusphere-2026-3557
Preprint. Discussion started: 26 June 2026

all members, and the variance metric provides a natural bridge to the percentile-based precipitation composite approach used in this study.

Storm track activity is thus quantified using the 24-hour difference filter variance of the 250-hPa meridional wind component following Chang et al. (2012) and Wallace et al. (1988). For each day, the filtered quantity is:

$$vv = \overline{\{v(t + 24hr) - v(t)\}^2} \qquad (1)$$

where v is the meridional wind and vv is the variance statistic at each grid point. This filter has half-power points at periods of approximately 1.2 and 6 days, effectively isolating synoptic-scale variability. Monthly mean vv is computed and then averaged seasonally. We focus on DJF and JJA as the seasons of maximum and minimum storm track activity respectively (Chang et al., 2012), providing the widest dynamic range against which to assess climate-change-induced shifts. The method is applied at multiple pressure levels (250, 500, 700 hPa) to capture the vertical structure of storm tracks. While upper-, mid-, and lower-tropospheric levels are examined in the physical mechanism diagnostics (Sect. 2.3), results are presented primarily at 250 hPa, which captures the upper-tropospheric storm track core where ETC activity and projected changes are the largest (Hoskins and Hodges, 2002; Yin, 2005). Statistical significance of projected changes is assessed using a two-sample t-test at the 95% confidence level ($p < 0.05$). The multi-model mean (MMM) is computed by first averaging over ensemble members within each model to obtain the forced response, then averaging across models.

2.3 Physical mechanisms

To diagnose the physical mechanisms driving storm track changes, we compute three quantities following Geng and Sugi (2003). The maximum Eady Growth Rate (EGR; σ_u) quantifies baroclinicity:

$$\sigma_u = 0.31 \frac{|f|}{N} \frac{\partial u}{\partial z} \qquad (2)$$

where f is the Coriolis parameter, $\partial u/\partial z$ is the vertical wind shear, and N is the Brunt-Väisälä frequency (a measure of static stability). The vertical wind shear is approximated via the thermal wind relation as proportional to the meridional temperature gradient: $\partial u/\partial z \propto -\partial T/\partial y$. Changes in these quantities are computed as ensemble-mean differences between the future and historical periods, analysed separately for the North Atlantic (0°–60°W, 20°–80°N) and North Pacific (140°–220°E, 20°–80°N) basins.

The EGR and baroclinicity diagnostics are presented for MPI only in the main text, with equivalent results for CanESM5 provided in the Supplement (Figs. S2–S3). This choice reflects two practical considerations: first, the multi-level daily pressure data required for these diagnostics were fully available only for MPI and CanESM5 from the MMLEA archive used in this study, precluding equivalent analysis for EC-Earth3; second, MPI and CanESM5 span opposite ends of the ECS range (2.8 K and 5.6 K respectively), such that they span the model spread. The robustness of the mechanistic interpretation is further supported by the consistency of large-scale storm track responses across all three models demonstrated in Sect. 3.2, which suggests that the physical mechanisms diagnosed from MPI are not model-specific but reflect a broader multi-model signal.

https://doi.org/10.5194/egusphere-2026-3557
Preprint. Discussion started: 26 June 2026

2.4 Internal variability quantification

To separate forced changes from internal variability, we follow García-Martínez and Bollasina (2021) and Rivosecchi et al. (2024). Since all ensemble members share identical external forcing but differ only in their initial conditions, differences among members reflect internal variability alone, while the ensemble mean isolates the externally forced response. The forced response is defined as the ensemble mean change; while internal variability is characterised by the spread across ensemble members. The fractional contribution of internal variability (IV) to the total projected change is estimated as:

$$IV\ (\%)\ =\ \sigma\ \times\ 100\ /\ (|\mu|\ +\ \sigma)\quad (3)$$

where μ is the ensemble mean change (the forced signal) and σ is the standard deviation across members (the noise). The spread in future outcomes is also characterised using the 5th–95th percentile range across ensemble member changes, constructed by computing the ensemble mean plus and minus two inter-member standard deviations.

2.5 Precipitation composite analysis

To link storm track changes to precipitation impacts, we use a percentile-based spatial composite approach, applied consistently across all ensemble members using historical percentile thresholds. This enables the contribution of ETCs at different intensity levels to projected precipitation changes to be quantified across the full NH. It thereby extends the Europe-focused analysis of Chang et al. (2022) to the Pacific domain and explicitly partitions storm-track-driven from residual precipitation changes, providing a more complete picture of how ETC-associated flooding risk may evolve under each scenario. Following Yau and Chang (2020), we define high-variance days as those when the basin-averaged vv exceeds its 95th percentile (representing intense ETCs), and moderate-variance days as those within the 25th–75th percentile range. Percentile thresholds are computed from the historical period vv averaged over the Atlantic (0°–60°W, 20°–80°N) and Pacific (140°E–220°E, 20°–80°N) and are then applied to composite daily precipitation over extended regions including adjacent land areas (Pacific: 120°E–105°W; Atlantic: 105°W–60°E; both 20°–80°N).

The fraction of total forced precipitation change attributable to storm track variability (f_{storm}) is defined following McKenna and Maycock (2022):

$$f_{storm}\ =\ \Delta P_{storm}\ /\ (\Delta P_{total}\ +\ \varepsilon)\quad (4)$$

where ΔP_{storm} is the precipitation change on high- or moderate-variance days, ΔP_{total} is the total forced precipitation change, and ε is a small positive number to avoid division by zero. Regions where $f_{storm} > 0.70$ indicate areas where more than 70% of the total precipitation change is attributable to storm track activity.

As with the mechanism diagnostics, the precipitation composite analysis is presented primarily for MPI in the main text, with CanESM5 results provided in the Supplement (Figs. S5, S7). MPI and CanESM5 span the lower and upper bounds of the model ECS range, ensuring that the composite results presented reflect both the weakest and strongest plausible responses. The two models show generally consistent spatial patterns, differing only in magnitude as expected from their ECS difference, providing confidence that the results are representative of the broader model ensemble.

https://doi.org/10.5194/egusphere-2026-3557
Preprint. Discussion started: 26 June 2026

3 Results

3.1 Present-day storm track climatology and model evaluation

ERA5 reanalysis for 1984–2014 reveals two distinct maxima in *vv* at 250 hPa, one over the central-to-eastern North Pacific (160°E–155°W, 30–60°N) and one over the North Atlantic (155°W–0, 35–65°N; Fig. 1a, b). This level is used throughout to represent the storm track core, where synoptic-scale meridional wind variance is largest and the forced signal is most pronounced (Hoskins and Hodges, 2002; Yin, 2005): Consistent with the established climatology (Hoskins and Hodges, 2019), DJF storm tracks are substantially stronger than during JJA, with peak *vv* values reaching approximately 450 $m^2 s^{-2}$ in winter versus ~300 $m^2 s^{-2}$ in summer.

The CMIP6 MMM reproduces the observed storm track climatology reasonably well but exhibits systematic biases (Fig. 1c, d). During DJF, the Atlantic storm track is overestimated (by up to ~100 $m^2 s^{-2}$) over the western Atlantic and Europe, and underestimated (~40 $m^2 s^{-2}$) over the Nordic Sea. The Atlantic bias has been attributed to a southward displacement of the simulated Atlantic jet stream (Harvey et al., 2020). The Pacific DJF bias is of opposite sign, with underestimation of up to 90 $m^2 s^{-2}$ over the central-to-eastern basin and a slight overestimation in the northern basin. Unlike the Atlantic case, this bias is more complex in structure and may reflect the difficulty of models in representing the midwinter minimum in storm track activity (Park and Lee, 2020). During JJA, the MMM is consistently weaker than ERA5 across the 40°–50°N band in both basins, with the most pronounced underestimation over the Atlantic. These biases are consistent in sign and magnitude with those documented across CMIP3, CMIP5, and CMIP6 by Harvey et al. (2020), confirming that they represent a pervasive feature across climate model generations rather than a deficiency specific to the three models selected here. As the analysis focuses on projected changes rather than absolute climatological values, and given that the bias patterns are broadly stationary between the historical and future periods, the biases do not materially affect the interpretation of the forced storm track response.

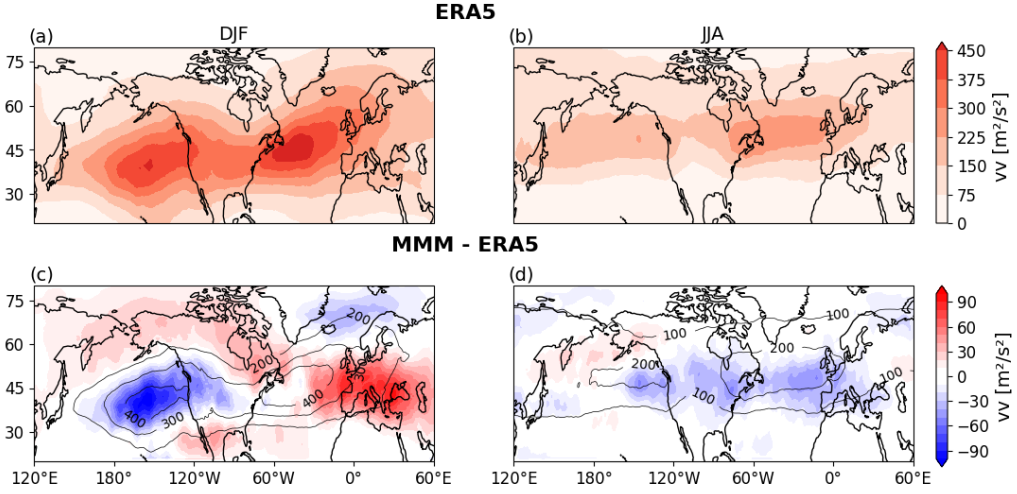

Figure 1. DJF and JJA 1984-2014 storm tracks at 250 hPa represented as *vv* (units: $m^2 s^{-2}$), from (a, b) ERA5, and (c, d) CMIP6 multimodel (EC-Earth3, CanESM5, and MPI) mean minus ERA5 differences. The contours in (c, d) represent the corresponding multimodel mean *vv* climatology (contour intervals: 100 $m^2 s^{-2}$). The left column is DJF, and the right column is JJA.

https://doi.org/10.5194/egusphere-2026-3557
Preprint. Discussion started: 26 June 2026

3.2 Projected changes in storm tracks

3.2.1 Spatial patterns

Figure 2 shows the projected DJF and JJA storm track changes at 250 hPa for the individual models and the MMM under both scenarios. All three models agree that storm tracks strengthen and shift poleward in DJF, in both the Atlantic and Pacific, with the Atlantic response directed more toward the northeast. The response is stronger under SSP5-8.5 than SSP2-4.5 in all models, confirming that the magnitude of the projected changes scales with both the level of anthropogenic forcing and the associated degree of global warming.

The strongest DJF response occurs in CanESM5 under SSP5-8.5 (Fig. 2f), where vv increases by up to approximately 100 $m^2 s^{-2}$. This increase extends across the Pacific basin and into northern North America above ~45°N, and approximately 50°–60°N in the Atlantic. EC-Earth3 shows a somewhat weaker and more spatially confined strengthening, concentrated mainly over the northern Pacific, with a weaker response over western Europe and eastern North America (Fig. 2b). MPI shows a broadly similar spatial pattern over the Pacific, but with a notable strengthening over the northern parts of North America rather than the more zonally confined Pacific-centred response seen in EC-Earth3 (Fig. 2j). The equatorward decrease in vv is evident in all models under SSP5-8.5, though this feature is less apparent in MPI under SSP2-4.5 (Fig. 2i). These inter-model differences are consistent with the differing ECS values: MPI, with the lowest ECS (2.8 K), produces the weakest and most localised response, while CanESM5, with the highest ECS (5.6 K), generates the strongest changes.

In JJA, the poleward shift seen in DJF is less evident, and the dominant projected response is a broad weakening of vv in the 45°–60°N latitude band across both the Atlantic and Pacific (Fig. 2, lower rows). The response is again stronger under SSP5-8.5 than SSP2-4.5. EC-Earth3 shows the largest JJA weakening, reaching up to ~100 $m^2 s^{-2}$ under SSP5-8.5. MPI again produces the most muted response, with substantial weakening confined mainly to the western portions of both basins (Figs. 2k, l). The projected changes are statistically significant at the 95% level in regions of model agreement across both seasons.

The range of individual ensemble member outcomes is illustrated in Figure 3 as the ensemble mean ± two inter-member standard deviations, representing the 5th–95th percentile spread. This framing allows a quantification of projection uncertainty and an identification of regions where the forced signal is robust across the plausible range associated with internal variability.

In DJF under SSP2-4.5, the poleward strengthening seen in the ensemble mean is not consistently projected across all plausible realisations: the lower plausible limit (Fig. 3c) shows no clear poleward increase in vv, and even a decrease in storm track activity along the Norwegian and North Sea. This region was already flagged as uncertain in Figure 2, where results were not statistically significant and individual models disagreed on the sign of the change. The expected equatorward decrease at lower latitudes is also absent in the upper plausible limit (Fig. 3a). Under SSP5-8.5, the spread narrows: the poleward increase is projected even in the lower plausible limit over the Pacific (Fig. 3g), although it is considerably weaker than the ensemble mean and absent over the Atlantic. The Norwegian–North Sea decrease persists in the lower plausible limit under SSP5-8.5, though it is weaker and more spatially confined. These results indicate that projected DJF changes over the Pacific under SSP5-8.5 are the most consistent across the plausible range of internal variability, while Atlantic changes, particularly at high latitudes, remain subject to greater uncertainty.

https://doi.org/10.5194/egusphere-2026-3557
Preprint. Discussion started: 26 June 2026

317 In JJA, the projected weakening is found in both the upper and lower plausible limits under both scenarios
318 (Figs. 3b, d, f, h), reflecting greater robustness of the summer response. The JJA ensemble spread is substantially
319 smaller than in DJF: the upper plausible limit shows a slightly weaker and more spatially confined decrease, with a
320 slight poleward strengthening above approximately 60°N that is absent in the lower limit. The substantially smaller
321 JJA ensemble spread relative to DJF is consistent with the smaller contribution of internal variability to summer storm
322 track projections, as discussed further in Section 3.4.

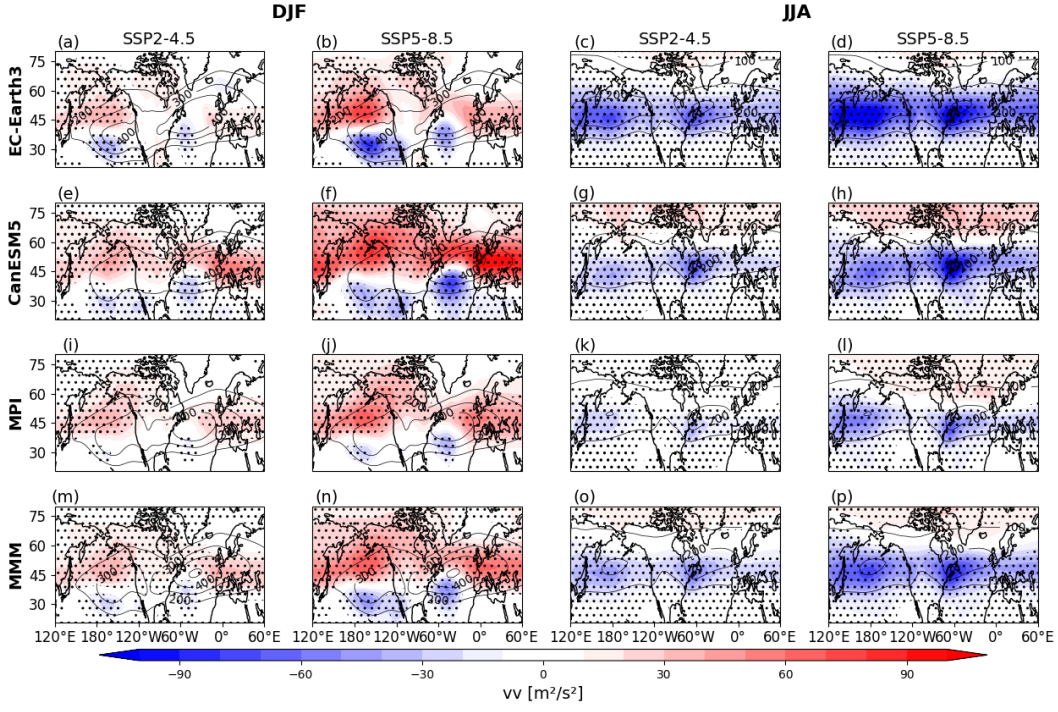

323

324 **Figure 2.** CMIP6 DJF and JJA *vv* changes (2070-2100 minus 1984-2014) at 250 hPa for SSP5-8.5 and SSP2-4.5 for
325 (a-l) individual models and (m-p) the multimodel mean (units: m^2s^{-2}). The dots represent (a-l) statistical significance
326 where P<0.05, and (m-p) model agreement on the sign of the change. The contours show the historical vv values
327 (contour interval: 100 m^2s^{-2}) for the (a-l) individual models and the (m-p) multimodel mean.
328

https://doi.org/10.5194/egusphere-2026-3557
Preprint. Discussion started: 26 June 2026

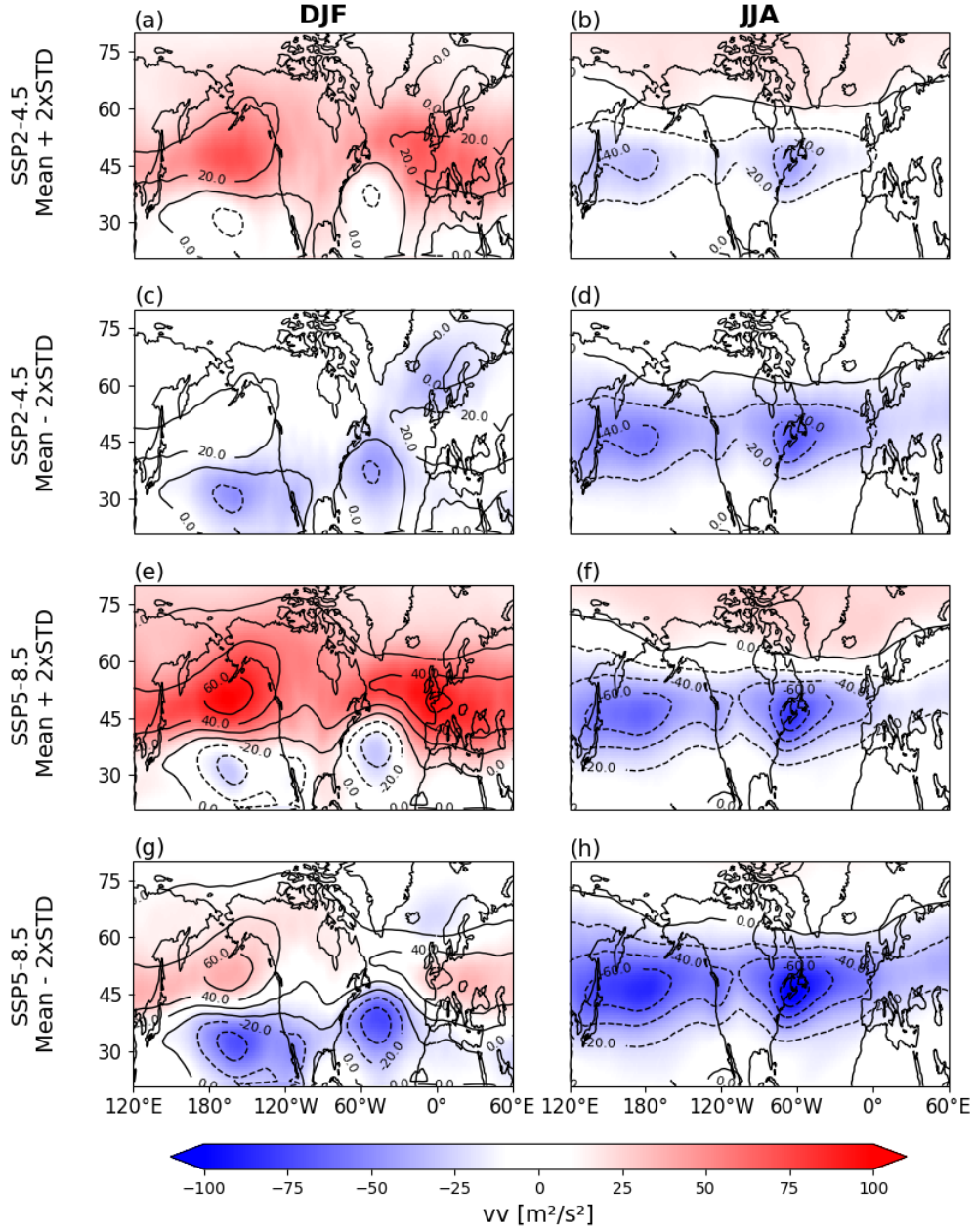

Figure 3. The 5-95% range of the simulated *vv* differences (2070-2100 minus 1984-2014) at 250 hPa for the MMM (a-d) SSP2-4.5 and (e-h) SSP5-8.5 scenarios. The 95% (mean plus two inter-member standard deviations) and the 5% (mean minus two inter-member standard deviations). The contour lines represent the ensemble mean (contour interval: 20 m^2s^{-2}).

https://doi.org/10.5194/egusphere-2026-3557
Preprint. Discussion started: 26 June 2026

3.2.2 Zonal mean changes and vertical structure

Figure 4 shows the DJF and JJA zonal mean vv for the individual models and the MMM over the two basins, with historical values from both ERA5 and the CMIP6 models alongside projected future changes. In the Atlantic, the DJF historical vv peaks at approximately 40°–50°N. ERA5 and CMIP6 show broadly similar values, though the CMIP6 models slightly overestimate the peak, most notably EC-Earth3, consistent with the positive bias identified in Section 3.1. In the future scenarios, all models agree on a dipole structure: decreasing vv from ~20° to 40°–45°N, transitioning to a peak of increasing values at approximately 50°–60°N. This is consistent with the spatial patterns in Figure 2. The peak values are larger and shifted further poleward under SSP5-8.5 than SSP2-4.5, and the inter-model spread is considerable, particularly for the future scenarios, indicating a non-negligible role of internal variability in determining the precise latitude and magnitude of the projected change.

In the Atlantic JJA, historical vv values are substantially smaller than in DJF, with the peak shifted slightly poleward to approximately 50°N, consistent with the seasonality of the Hadley Cell and reduced baroclinicity in summer. CMIP6 models generally underestimate ERA5 values, consistent with Figure 1d, with EC-Earth3 being an exception showing slightly larger values northward of the peak. In the future scenarios, a clear decrease is projected at approximately 45°N, larger in magnitude under SSP5-8.5 than SSP2-4.5. Poleward of this minimum, vv increases slightly, becoming weakly positive above ~60°N. The ensemble member spread is substantially smaller in JJA than in DJF, reinforcing the view that the projected summertime weakening is a robust feature of the forced response and is comparatively insensitive to internal variability.

The Pacific DJF historical vv is slightly weaker than the Atlantic and peaks further south, at approximately 40°N. CMIP6 models underestimate ERA5 values in the Pacific, consistent with the negative bias in Section 3.1, and this is particularly pronounced in CanESM5. The projected future changes are qualitatively similar to the Atlantic: a dip in vv at approximately 35°–40°N transitions to a peak of increasing values near 50°N, with larger changes under SSP5-8.5. The inter-member spread is again large in DJF, indicating that the magnitude of the Pacific response is subject to considerable internal variability. In JJA, individual model responses relative to ERA5 show more spread than in the Atlantic: EC-Earth3 shows higher historical values than ERA5, CanESM5 lower, and MPI is approximately consistent. The projected weakening again peaks at 45°–50°N with a slight poleward increase, and the ensemble spread is considerably smaller than in DJF, consistent with the Atlantic result.

The vertical structure of the projected changes is examined in Figure 5 using the MPI LE. While three models were analysed for the spatial patterns in Section 3.2.1, MPI is used here as a representative case to explore the vertical structure in detail; the analysis has also been performed using CanESM5, which shows comparable patterns of change at larger magnitudes (Fig. S1). In the Atlantic during DJF, a clear increase in vv is found from approximately 400 hPa upwards under SSP2-4.5 (Fig. 5c), peaking between 300 and 200 hPa, slightly higher in the atmosphere than the historical maximum. Under SSP5-8.5 (Fig. 5d), the strengthening extends downward to ~500 hPa and is at its strongest between 250 and 200 hPa, again displaced upward relative to historical values. In the Atlantic during JJA, the dominant response is a weakening spanning 600 to 150 hPa under SSP2-4.5 (Fig. 5g), with a slight compensating increase poleward of the weakening between 300 and 200 hPa. Under SSP5-8.5 (Fig. 5h), the weakening deepens to 800 hPa and the poleward increase extends from 400 to 150 hPa. In the Pacific during DJF, vv increases from ~500 hPa

https://doi.org/10.5194/egusphere-2026-3557
Preprint. Discussion started: 26 June 2026

upwards under SSP2-4.5 (Fig. 5a), peaking between 300 and 200 hPa, higher than the historical maximum, while under SSP5-8.5 (Fig. 5b) the response is strongly enhanced but the vertical position of the track core remains similar. In the Pacific during JJA, the weakening occurs from approximately 600 to 150 hPa under SSP2-4.5, with a peak around 250 hPa (Fig. 5e), and a slight poleward increase between 300 and 200 hPa. Under SSP5-8.5 (Fig. 5f), the weakening deepens substantially, spanning from ~900 to 130 hPa with a peak at approximately 250 hPa, and the poleward increase is slightly enhanced, extending from 400 to 150 hPa. The upward migration of the storm track core in both basins and seasons is consistent with the rising tropopause and enhanced upper-tropospheric baroclinicity expected under global warming (Yin, 2005; Shaw et al., 2016). Although the vertical structure analysis is based solely on MPI, the consistency in large-scale storm track responses across all three models in Section 3.2.1 suggests that these changes are not model-specific but are likely robust features of the multi-model response.

Comparing the two basins, the Pacific exhibits larger absolute projected changes than the Atlantic in the MMM and in two of the three individual models (EC-Earth3 and MPI), while CanESM5, the highest-ECS model, produces stronger Atlantic changes. This is noteworthy given that the Atlantic is the historically more active storm track basin (Harvey et al., 2020), and that the known CMIP6 biases, featuring an overestimation of the Atlantic tracks and an underestimation in the Pacific basin, would, if anything, would be expected to inflate projected Atlantic changes relative to the Pacific. The fact that the Pacific nonetheless shows larger projected changes in most models is suggestive of it being intrinsically more sensitive to anthropogenic forcing, a finding that warrants further investigation.

https://doi.org/10.5194/egusphere-2026-3557
Preprint. Discussion started: 26 June 2026

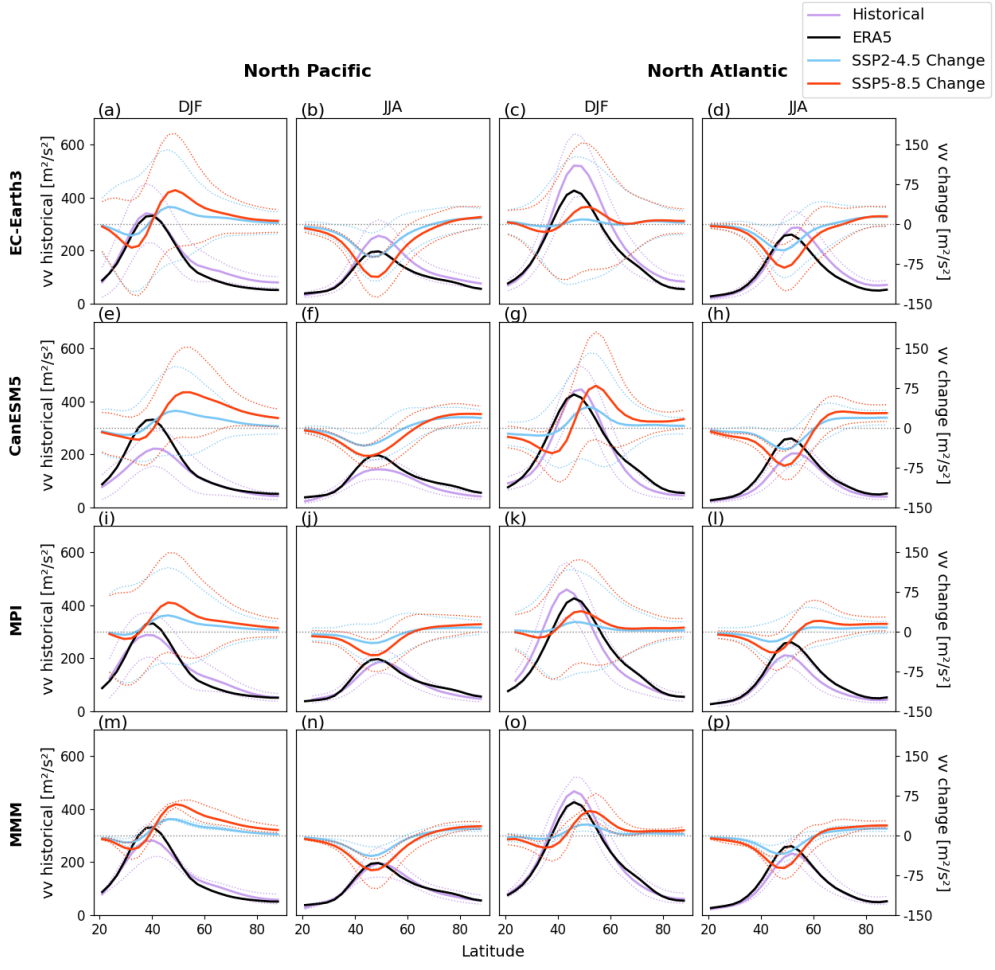

Figure 4. Historical values (1984-2014) and future changes (2070-2100 minus 1984-2014) of DJF and JJA storm tracks at 250 hPa for the Atlantic and the Pacific, defined as (0-60°W, 20-90°N) and (140°E-140°W, 20-90°N), respectively. The subplots in (a-l) show the ensemble mean of individual CMIP6 large ensemble models and in (m-p) the multimodel mean of these models. The individual models include (a-d) EC-Earth3, (e-h) CanESM5, and (i-l) MPI. The lavender and black lines represent CMIP6 and ERA5 historical *vv* values (units: m^2s^{-2}), respectively, and the values correspond to the primary y axis. Blue and red lines represent the future changes for the SSP2-4.5 and SSP5-8.5 CMIP6 scenarios (units: m^2s^{-2}), respectively, and values correspond to the secondary y axis. The dotted lines represent (a-l) one standard deviation of the ensemble member values, and (m-p) the minimum and maximum values of the ensemble mean for the individual models.

https://doi.org/10.5194/egusphere-2026-3557
Preprint. Discussion started: 26 June 2026

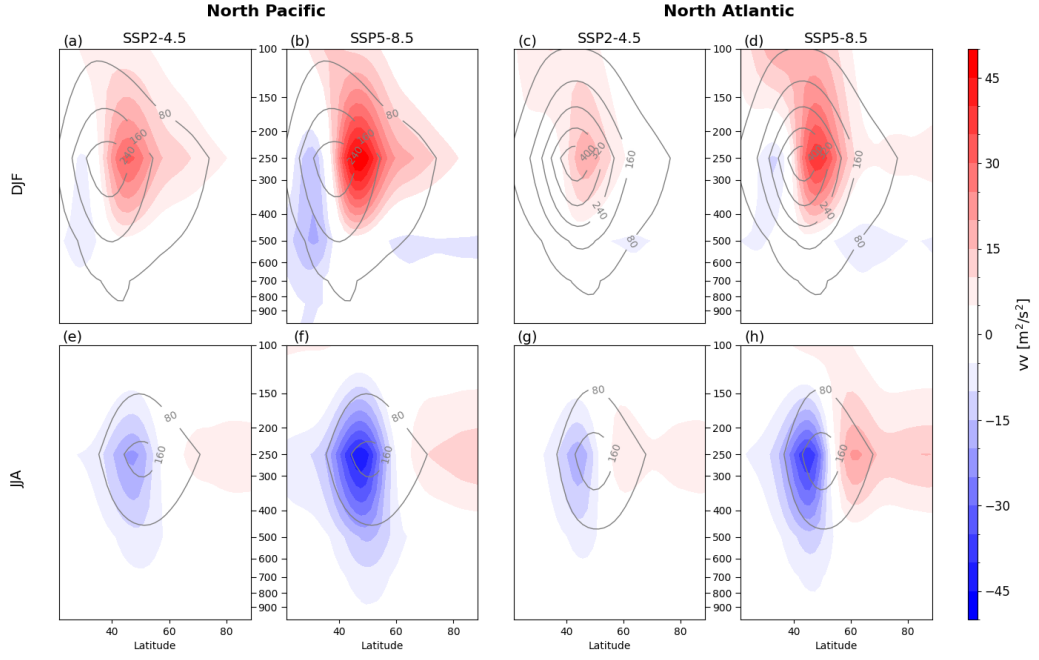

Figure 5. The MPI zonal mean DJF and JJA vv changes (2070-2100 minus 1984-2014) for SSP5-8.5 and SSP2-4.5 over the Atlantic and Pacific, using MPI large ensemble. The contour lines show the historical (1984-2014) zonal mean vv (contour interval: 80 m^2s^{-2}).

3.3 Physical mechanisms

The existence of ETCs is fundamentally linked to atmospheric baroclinicity. Previous studies have examined how anthropogenic climate change will alter this baroclinicity and thereby modify storm tracks (e.g., Geng and Sugi, 2003; Yin, 2005), finding that the projected poleward and upward shift in storm tracks is associated with a corresponding poleward shift and upward expansion of the midlatitude baroclinic regions (Yin, 2005). However, baroclinicity alone cannot account for all of the projected changes (Geng and Sugi, 2003), and static stability must also be considered. Figures 6 and 7 therefore show the projected changes in Eady Growth Rate (EGR; Figs. 6, 7a–d), as a measure of baroclinicity, together with the three factors that contribute to changes in EGR: the Brunt–Väisälä frequency (N; Figs. 6, 7e–h), the vertical wind shear (Figs. 6, 7i–l), and the meridional temperature gradient (Figs. 6, 7m–p), using the MPI LE. CanESM5 shows spatially comparable patterns at larger magnitudes consistent with its higher ECS (Figs. S2-S3); the justification for this single-model presentation is given in Section 2.3. Figure 6 shows results for SSP2-4.5 and Figure 7 for SSP5-8.5; as the spatial patterns are broadly similar between scenarios, they are discussed together, with differences in magnitude noted where relevant.

The present-day climatological distribution of EGR differs between the two basins. In the Pacific, there is a clear peak of ~1.0 day^{-1} at approximately 30°N and 400 hPa during DJF (Figs. 6, 7a), with a secondary increase equatorward reaching ~0.6 day^{-1} at 30°–40°N and 150–100 hPa. During JJA, values are substantially smaller, peaking at ~0.4 day^{-1} at approximately 50°N between 300 and 400 hPa (Figs. 6, 7b). In the Atlantic, historical EGR values are

https://doi.org/10.5194/egusphere-2026-3557
Preprint. Discussion started: 26 June 2026

smaller overall, with a peak of ~1.0 day^{-1} near the surface at high latitudes during DJF (Figs. 6, 7c), likely influenced by surface processes, and a secondary peak of ~0.6 day^{-1} at 40°N and 500–400 hPa. During JJA, the Atlantic EGR peak is shifted poleward to ~50°N and 600–300 hPa, reaching ~0.4 day^{-1} (Figs. 6, 7d).

The projected changes in EGR are well correlated with changes in vertical wind shear and the meridional temperature gradient, particularly in the Atlantic. Two distinct thermodynamic mechanisms operate at different levels in the troposphere. Near the surface, polar amplification, the preferential warming of the Arctic relative to lower latitudes, driven by snow and ice albedo feedbacks (Holland and Bitz, 2003), weakens the lower-tropospheric meridional temperature gradient in the midlatitudes, reducing low-level baroclinicity, which tends to weaken the storm tracks. In the mid-to-upper troposphere, however, enhanced tropical warming relative to higher latitudes through moist-adiabatic adjustment (Held, 1993; Shaw et al., 2016) strengthens the upper-level meridional temperature gradient between the tropics and the poles and, through the thermal wind relation, increases vertical wind shear and upper-level baroclinicity. This upper-level response favours a poleward shift and upward intensification of the DJF storm track core. The net DJF response thus reflects the dominance of the upper-tropospheric mechanism over the near-surface reduction in baroclinicity, consistent with the upward displacement of the EGR increase seen in Figures 6 and 7. The response under SSP5-8.5 is considerably larger than under SSP2-4.5, consistent with greater overall warming and stronger polar and amplified upper-tropospheric temperature changes at higher emission levels. It should be acknowledged that the temperature gradient changes diagnosed here reflect the combined effect of greenhouse gas increases and reductions in anthropogenic aerosol emissions, both of which contribute to future NH warming. The relative contribution of aerosol forcing to the projected baroclinicity changes, particularly over the Atlantic sector where historical aerosol loading has been largest, is not explicitly separated in this analysis and represents a source of uncertainty in the mechanistic attribution presented here.

In the Atlantic during DJF, a clear increase in EGR is found at approximately 400–200 hPa and 20°–50°N (Figs. 6, 7c), extending down towards the surface around 30°N. There is a corresponding decrease in EGR extending from ~500 hPa towards the surface between 50° and 80°N, consistent with the overall reduction in lower-tropospheric baroclinicity driven by the competing effects of polar amplification and reduced meridional temperature gradients. During JJA, an increase in EGR is found but confined to 300–200 hPa and shifted poleward relative to DJF (Figs. 6, 7d); this localised upper-level increase is likely associated with the rising tropopause and does not offset the net weakening, which is evident at both lower and higher pressure levels. In the Pacific during DJF, the pattern is broadly similar to the Atlantic, but the EGR increase is stronger poleward and extends further towards the poles in the upper troposphere (Figs. 6, 7a). A similar inter-basin asymmetry is evident in JJA, where the equatorward EGR increase in the Pacific occurs at higher levels (~200 hPa), while poleward of this the increase shifts to lower pressure levels (400–250 hPa; Figs. 6, 7b).

While the meridional temperature gradient and vertical wind shear explain much of the projected EGR change, particularly in the Atlantic, there are regions where these factors alone are insufficient. In these areas, changes in static stability (N) provide the complementary explanation. Figures 6 and 7e–f show an overall decrease in N towards the poles and at 300–150 hPa in the midlatitudes under both scenarios. In JJA, the spatial pattern of decreasing N closely mirrors that of the EGR increase (Fig. 6 and Figs. 7b, d): the band of increasing baroclinicity stretches upward

https://doi.org/10.5194/egusphere-2026-3557
Preprint. Discussion started: 26 June 2026

equatorward and descends towards the pole, while below this band a decrease in EGR is co-located with an increase in N from ~300 hPa towards the surface. This seasonal difference in the relative importance of static stability versus the meridional temperature gradient — with N playing a larger role in JJA — is consistent with Yin (2005) and Geng and Sugi (2003), and explains why the summer storm track response (a broad weakening) is physically distinct from the winter response (a poleward intensification).

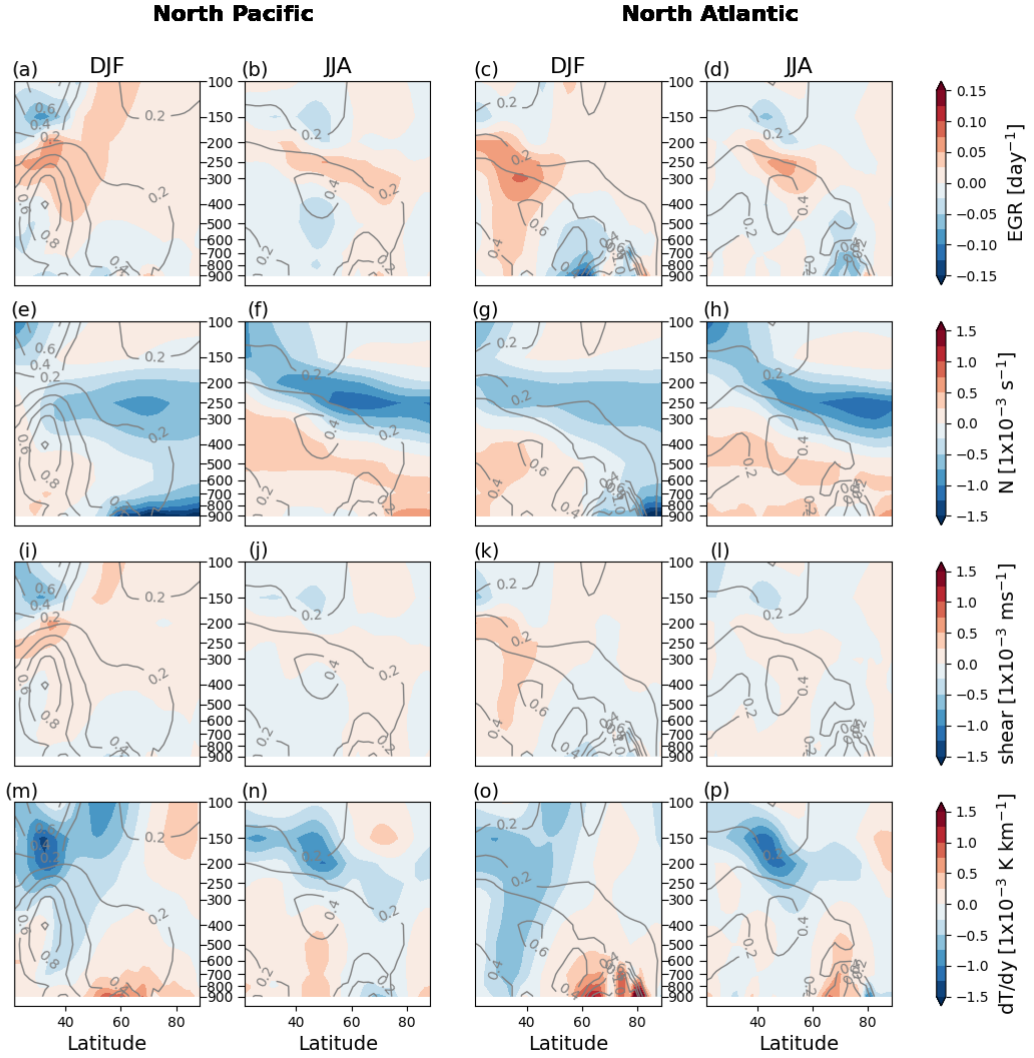

Figure 6. The DJF and JJA changes (2070-2100 minus 1984-2014) for SSP2-4.5 over the Atlantic and Pacific for (a-d) maximum Eady growth rate (units: day^{-1}), (e-h) Brunt-Vaisala frequency (units: s^{-1}), (i-l) vertical wind shear (units: ms^{-1}), and (m-p) meridional temperature gradient (units: K km^{-1}), using MPI large ensemble. The contours show 1984-2014 zonal means of maximum Eady growth rate (contour interval: 0.2 day^{-1}).

https://doi.org/10.5194/egusphere-2026-3557
Preprint. Discussion started: 26 June 2026

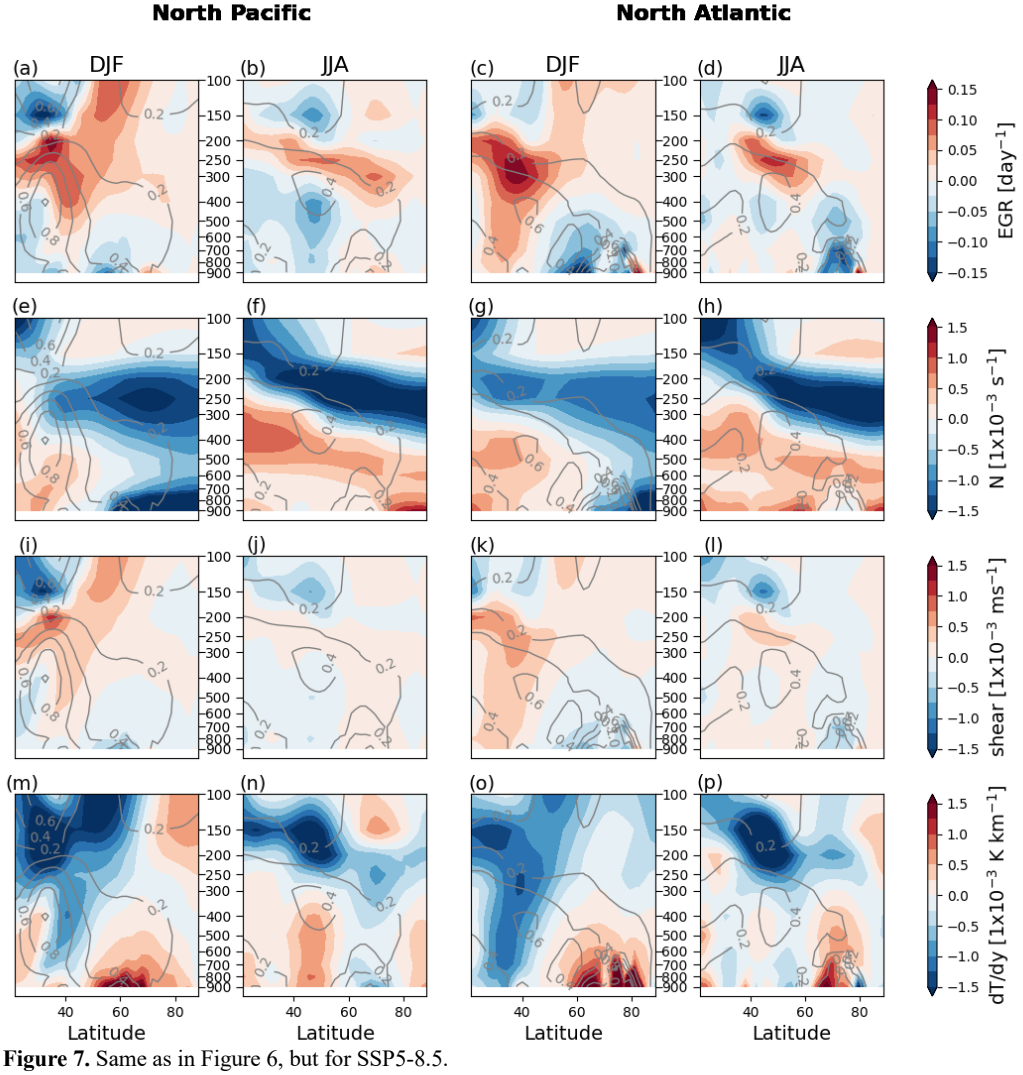

Figure 7. Same as in Figure 6, but for SSP5-8.5.

3.4 Role of internal variability

LE simulations sample a wide range of plausible future outcomes, enabling a robust separation of externally forced changes from internal climate variability and thereby clarifying the relative contributions of anthropogenic forcing and natural fluctuations.

Figure 8 displays the relative contribution of internal variability (RIV, %) to projected storm track changes, where 100% indicates that the total change is driven by internal variability and 0% indicates that external forcing is

https://doi.org/10.5194/egusphere-2026-3557
Preprint. Discussion started: 26 June 2026

the sole driver. The RIV is computed only where historical vv exceeds 100 $m^2 s^{-2}$ and the projected change exceeds 10 $m^2 s^{-2}$, in order to focus the analysis on the active storm track regions and avoid artefacts from near-zero changes.

There are clear differences between seasons and scenarios. It is important to note that the high RIV values reported here do not imply that internal variability is large in absolute terms, but rather that the externally forced signal, while present, remains relatively modest compared to the natural spread of possible outcomes, particularly under SSP2-4.5 where anthropogenic forcing is weaker. During DJF, RIV is substantially higher under SSP2-4.5 (Fig. 8a), with internal variability accounting for approximately 80–90% of the total projected change across both basins, reflecting the comparatively weak forced signal at this emission level rather than an unusually large magnitude of internal variability. Under SSP5-8.5 (Fig. 8b), the RIV is considerably reduced to approximately 70%, particularly over the Pacific, the southern Atlantic, and Europe, where the stronger externally forced signal increasingly dominates.

A similar but seasonally modulated pattern is found during JJA: RIV is generally lower than in DJF for both scenarios, with internal variability contributing around 70% under SSP2-4.5 (Fig. 8c) and decreasing further to approximately 50–60% under SSP5-8.5 (Fig. 8d). Notably, the areas of most reduced RIV correspond to the regions where projected storm track changes are largest, as illustrated by the white contour lines in Figure 8, confirming that the forced signal is strongest precisely where the storm track response is most prominent.

These results indicate that internal variability remains a substantial source of uncertainty even at end-of-century timescales, particularly during DJF and under SSP2-4.5. Under SSP2-4.5 in DJF, a subset of members shows no poleward shift or even a slight equatorward displacement, highlighting that single-member projections can be misleading under lower-forcing scenarios. Conversely, the consistently lower RIV during JJA, and the near-universal agreement on the weakening signal across ensemble members, provides greater confidence in the summer storm track projections under both scenarios. This underlines the importance of LE approaches for characterising the full range of plausible outcomes and for correctly attributing projected changes to their forcing.

https://doi.org/10.5194/egusphere-2026-3557
Preprint. Discussion started: 26 June 2026

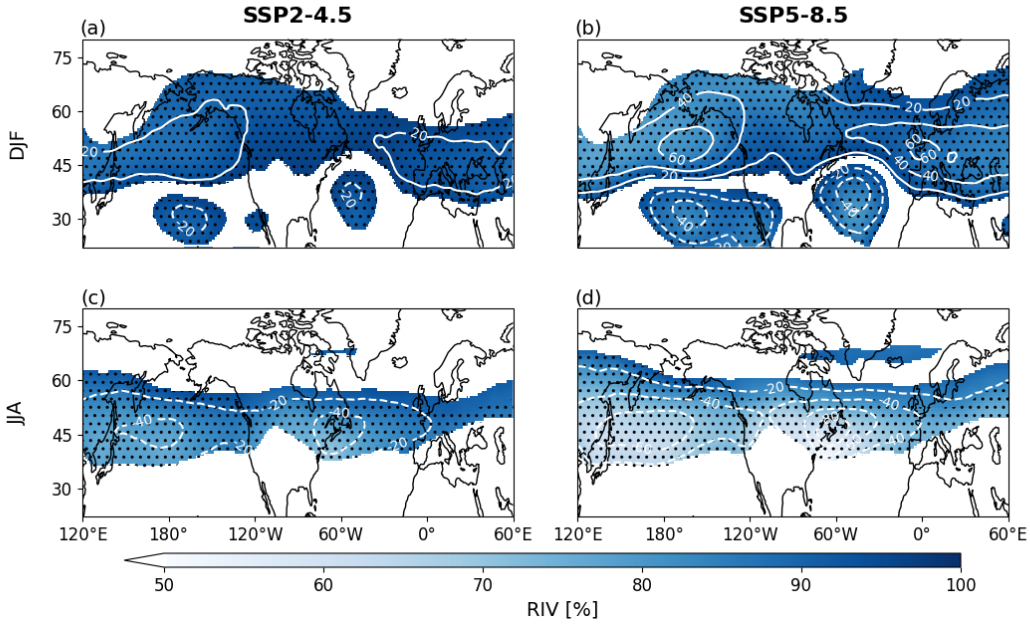

Figure 8. The relative contribution of internal variability (%) to the changes (2070-2100 minus 1984-2014) for (a-b) DJF and (c-d) JJA, for the MMM. The RIV is only plotted for historical *vv* values above 100 m^2s^{-2}, and all changes between -10 and 10 m^2s^{-2} are masked. The dots indicate the grid points where all three models agree on the sign of the change in vv. White contour lines indicate the change in *vv*, where dashed lines are negative (contour interval: 20 m^2s^{-2}).

3.5 Impacts on precipitation

Changes in Atlantic and Pacific storm tracks may cause significant impacts on future weather events, including extreme wind and precipitation. Figures 9 and 10 show the projected changes in *vv* and precipitation, respectively, on high- and moderate-variance days, using the MPI LE; the same analysis has been performed using CanESM5, which shows spatially consistent patterns at larger magnitudes (Fig. S4–5); the justification for presenting MPI as the primary model is given in Sect. 2.5.

During DJF on high-variance days under SSP2-4.5, storm tracks weaken in both the Atlantic and Pacific at approximately 30°–45°N (Fig. 9a), while a slight strengthening is found over Europe, the northern Pacific, and North America. During moderate-variance days, the westward Atlantic weakening persists alongside a weakening at ~30°N in the Pacific, while the strengthening over Europe and North America is still evident but clearly reduced; a slight strengthening over eastern Asia at approximately 45°N, not identified during high-variance days, is also found (Fig. 9c). The visible seam at approximately 105°W reflects the boundary between the Pacific and Atlantic basin masks as defined in the methodology. Under SSP5-8.5, all responses are stronger: the strengthening over Europe, the northern Pacific, and North America is more prominent on high-variance days (Fig. 9e), as is the equatorward weakening; these patterns are also evident during moderate-variance days, with an enhanced response over East Asia and northeast Asia and northern North America (Fig. 9g).

https://doi.org/10.5194/egusphere-2026-3557
Preprint. Discussion started: 26 June 2026

When comparing the storm track changes in Figure 9 to the corresponding precipitation composites in Figure 10, it is clear that the overall response to the poleward shift of DJF storm tracks is increasing precipitation poleward of the historical maximum, which lies at approximately 30°–40°N in both basins. In the Pacific under SSP2-4.5, precipitation increases from approximately 40° to 75°N on high-variance days (Fig. 10a), with a slight decrease around 30°N. In the Atlantic, increases are found in the eastern and western parts at approximately 45°–50°N and along the Norwegian Sea, while a decrease is projected off the northwest coast of the British Isles, a region of historical precipitation maximum, which is a robust and notable departure from the general poleward enhancement. During moderate-variance days, the same patterns are found but substantially weaker (Fig. 10c). Under SSP5-8.5, the response is considerably stronger, with a clear reduction in precipitation up to approximately 40°N and a robust poleward increase across both basins (Figs. 10e, g); the decrease off the British Isles is more evident during moderate-variance days in this scenario.

During JJA, the storm track responses are broadly similar to those in DJF but shifted poleward. Under SSP2-4.5, the most prominent changes on high-variance days are decreases in storm track activity in the central and western Pacific and in the western Atlantic, both at approximately 45°–55°N (Fig. 9b), alongside an increase over the northern Pacific that is less evident over the northern Atlantic. These findings are also evident during moderate-variance days but are less prominent (Fig. 9d). Under SSP5-8.5, storm tracks weaken at approximately 45°–50°N and strengthen poleward, especially over the northern Atlantic, Pacific, and North America (Fig. 9f). During moderate-variance days under SSP5-8.5, these signals are significantly weakened, with the main features being a weakening over the Atlantic with a strengthening above approximately 60°N, and a weakening over East Asia in the Pacific (Fig. 9h). The CanESM5 results show similar patterns of change to MPI but with a stronger magnitude (Fig. S4).

The corresponding JJA precipitation composites reveal a more spatially complex response than DJF. Under SSP2-4.5, precipitation increases over East Asia and the western Pacific on high-variance days (Fig. 10b), consistent with the historical precipitation hotspot in this region. As discussed in the f_{storm} analysis below, storm track variability accounts for a relatively small fraction of this increase, suggesting that other dynamical processes, beyond the scope of the present analysis, contribute substantially to precipitation changes in this region. A strong decrease is projected over central North America, with a slight decrease also over the southern Atlantic and western Europe. During moderate-variance days, the East Asia response spans a smaller area while the European increase covers a greater area (Fig. 10d). Under SSP5-8.5, the East Asia and northern Pacific increase is stronger, the central North America decrease is more pronounced, and strong decreases emerge over the southwestern Atlantic and western Europe, with stronger increases in both the southwest and southeast of North America (Fig. 10f). These signals are slightly weakened but remain prominent during moderate-variance days (Fig. 10h).

Across both seasons, storm track variability accounts for more than 70% of the forced precipitation change ($f_{storm} > 0.70$) over the northern Pacific and North America in DJF, confirming that the poleward storm track shift is the primary driver of precipitation change in these regions. Over Europe in DJF, f_{storm} is substantially lower, suggesting that other processes, possibly changes in the Atlantic jet stream position or blocking frequency, play a larger role. In JJA, f_{storm} is generally lower than in DJF, though storm track variability remains an important

https://doi.org/10.5194/egusphere-2026-3557
Preprint. Discussion started: 26 June 2026

contributor to the projected precipitation decreases over central North America and the central Atlantic, consistent with the weakening of ETC activity in these regions.

There are notable inter-model differences in precipitation response. CanESM5, with its higher ECS, projects substantially stronger precipitation enhancement poleward and greater increases over Europe and North America during DJF compared to MPI; these differences are particularly striking in the composite analyses (Fig. S5), where CanESM5 shows considerably stronger poleward enhancements. The total forced precipitation changes also differ substantially between models (Figs. S6-7), with the largest inter-model differences found over Europe and North America. These inter-model differences highlight the sensitivity of regional precipitation projections to model formulation, and with the internal variability results in Section 3.4, underscore the importance of utilising multiple LE models for robust climate impact assessment.

https://doi.org/10.5194/egusphere-2026-3557
Preprint. Discussion started: 26 June 2026

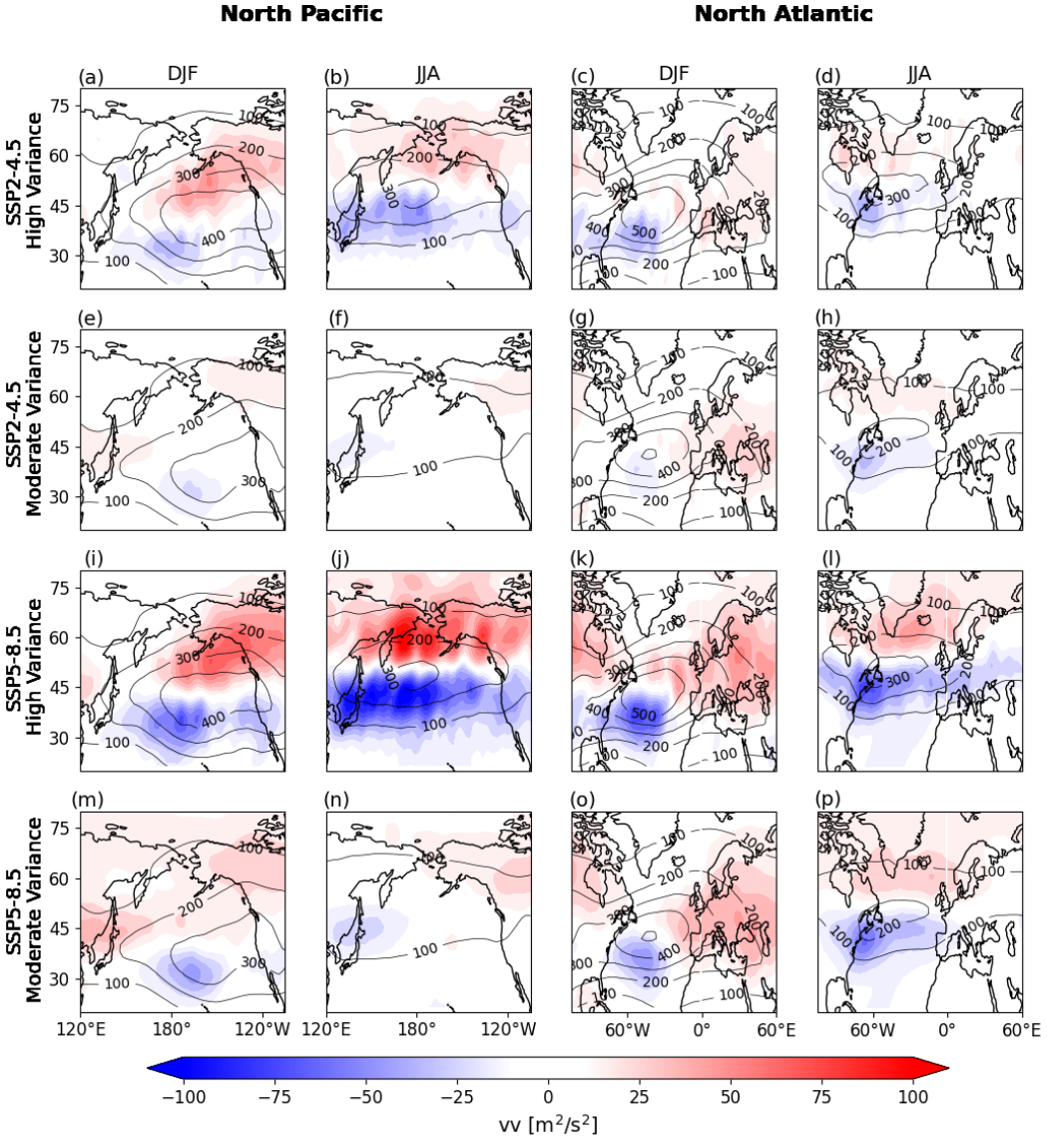

572

573 **Figure 9.** The MPI northern hemisphere storm tracks at 250 hPa during high-, and moderate-variance days for DJF
574 and JJA, using MPI large ensemble. The contour lines represent the historical storm track values (contour interval:
575 100 m^2s^{-2}).

576

https://doi.org/10.5194/egusphere-2026-3557
Preprint. Discussion started: 26 June 2026

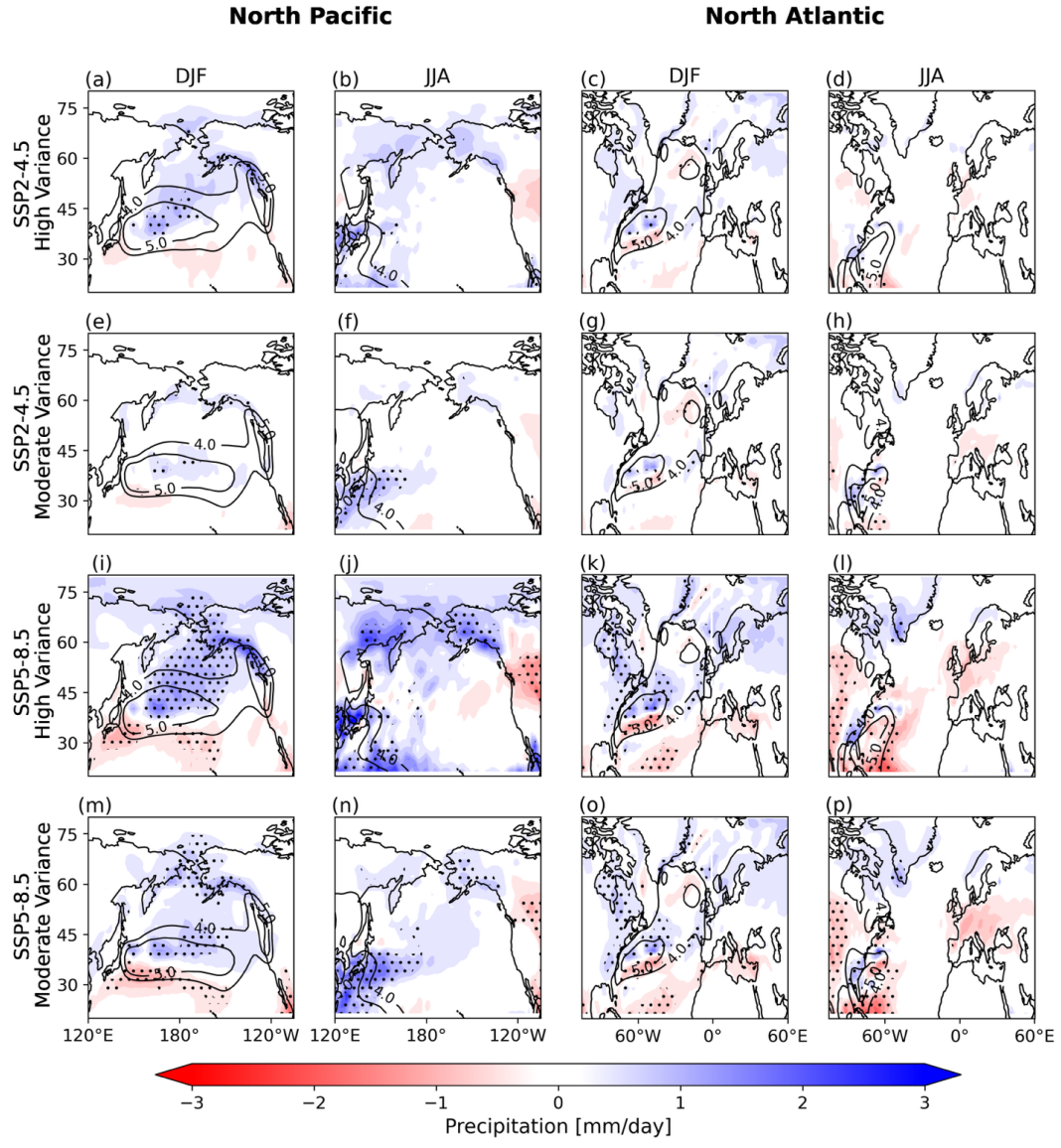

Figure 10. The MPI northern hemisphere precipitation during high-, and moderate-variance days for DJF and JJA, using MPI large ensemble. The dots indicate areas where more than 70% of the forced precipitation change is attributable to storm track variability. The contour lines represent the historical precipitation values (contour interval: 1.0 mm day^{-1}).

https://doi.org/10.5194/egusphere-2026-3557
Preprint. Discussion started: 26 June 2026

4 Discussion and Conclusions

We have investigated projected changes in Northern Hemisphere storm tracks and their precipitation impacts using LE CMIP6 simulations from EC-Earth3, CanESM5, and MPI under SSP2-4.5 and SSP5-8.5. The main conclusions are as follows:

(i) DJF storm tracks shift poleward and intensify under both scenarios, driven by the competing effects of near-surface polar amplification and tropical upper-tropospheric warming, with the latter dominating through enhanced upper-level wind shear and baroclinicity that shift baroclinic instability toward higher latitudes. This poleward shift enhances precipitation at latitudes poleward of ~45°N, with the Pacific and North America being most directly storm-track-controlled.

(ii) JJA storm tracks weaken across both the Pacific and Atlantic basins, driven primarily by changes in static stability (Brunt–Väisälä frequency) rather than the temperature gradient. This weakening contributes to decreased midlatitude precipitation that partially offsets thermodynamically driven increases from enhanced atmospheric moisture.

(iii) Internal variability plays a prominent role in DJF projections, particularly under SSP2-4.5, where the forced signal is weaker and ensemble members span a wide range of outcomes including cases with no detectable poleward shift. The contribution of internal variability is substantially reduced during JJA and under SSP5-8.5, where the externally forced signal dominates.

(iv) Inter-model spread, linked primarily to differing ECS values, is substantial in both the magnitude and regional detail of projected changes, particularly for precipitation. CanESM5 consistently projects stronger responses than MPI, with EC-Earth3 intermediate. This sensitivity to ECS underlines the importance of multi-model LE frameworks for robust climate impact assessment.

These results advance the quantitative understanding of the forced and internally variable components of future NH storm track change, and provide a comprehensive basis for evaluating ETC behaviour relevant to climate adaptation planning.

The projected DJF poleward intensification and JJA weakening are broadly consistent with prior literature across CMIP3, CMIP5, and CMIP6 (Yin, 2005; Chang et al., 2012; Harvey et al., 2020; Priestley and Catto, 2022), and the stronger response under SSP5-8.5 aligns with the scenario-dependence documented by Priestley and Catto (2022). The recently attributed anthropogenic weakening of JJA storm tracks (Chemke and Coumou, 2024; Shaw et al., 2024) is consistent with our end-of-century projections showing a ~15–25% decline in JJA vv across all models and scenarios. The CMIP6 model biases identified in Section 3.1 — overestimation of the Atlantic storm track and underestimation of the Pacific — are consistent with those documented across successive CMIP generations by Harvey et al. (2020), confirming they are a long-standing feature of the model class rather than deficiencies specific to the three models used here. These biases affect the reliability of absolute projected magnitudes, particularly over the Pacific, and continued evaluation of model performance against reanalysis is therefore essential. Our basin-resolved physical mechanism analysis extends the NH-integrated work of Geng and Sugi (2003) and Yin (2005), confirming that DJF EGR changes are primarily driven by changes in the meridional temperature gradient and vertical wind shear, while JJA changes are dominated by static stability. The DJF result reflects the dominance of tropical upper-

https://doi.org/10.5194/egusphere-2026-3557
Preprint. Discussion started: 26 June 2026

tropospheric warming over near-surface polar amplification in determining the net baroclinicity change; the JJA result, where static stability plays the leading role, explains why the summer response is physically distinct from winter and why the seasonal contrast between DJF intensification and JJA weakening is likely to Chang et al. (2022), who found analogous DJF precipitation increases near the British Isles and northern Europe and JJA decreases over central Europe, while our composite approach additionally quantifies the fraction of these changes attributable to storm track variability, demonstrating that the Pacific and North America are more directly storm-track-controlled than Europe in DJF. In JJA, the Atlantic precipitation response agrees more closely with storm track changes than the Pacific: increases over Greenland and northern Scandinavia are consistent with storm track strengthening in those regions, while the precipitation decrease across much of Europe and North America aligns with the findings of Chang et al. (2022) regarding weakened JJA storm tracks. Over the Pacific in JJA, the weaker correlation between precipitation changes and storm track variability suggests that other processes contribute substantially to precipitation changes in that region.

A key methodological distinction of this study is the use of LE simulations with many members per model rather than a single member from many models. This design enables a robust estimate of the forced response and an explicit quantification of internal variability within each model, a trade-off that is particularly valuable for assessing projection uncertainty at regional scales. Our basin-resolved mechanism analysis reveals quantitative differences between the Atlantic and Pacific that are obscured in NH-integrated diagnostics, including stronger upper-level EGR changes in the Atlantic and more pronounced mid-tropospheric changes in the Pacific during DJF. The percentile-based composite approach additionally allows explicit attribution of precipitation changes to storm track variability via the f_{storm} metric, a methodological advance relative to studies using only seasonal mean activity indices. An important and somewhat unexpected finding from the composite analysis is that the storm track response on high-variance days in JJA bears a closer resemblance to DJF than to the JJA seasonal mean, showing a poleward strengthening rather than the broad weakening seen in the seasonal mean. This suggests that during intense ETC events, the influence of the seasonal cycle diminishes, and that when such events occur in summer they are governed by dynamical processes more akin to those in winter. This finding also underlines the importance of considering moderate-intensity ETCs alongside the high-variance tail: moderate-variance days show significant contributions to precipitation changes under both scenarios, and focusing exclusively on extreme events would underestimate the total storm-track-driven precipitation response.

Inter-model differences, linked primarily to ECS, propagate throughout the results. MPI, with the lowest ECS (2.8 K), consistently projects the weakest storm track and precipitation changes; CanESM5, with the highest ECS (5.6 K), projects the strongest; EC-Earth3 (4.3 K) is intermediate. These differences reflect the models' differing cloud feedback representations (Maher et al., 2019; Virgin et al., 2021) and translate directly into differences in the projected meridional temperature gradient change and associated storm track response. They are particularly evident in the precipitation composites, where CanESM5 projects substantially stronger poleward enhancement and greater increases over Europe and North America during DJF, while MPI projects decreases in those same regions. These discrepancies highlight the sensitivity of regional projections to model formulation and underscore the importance of spanning a wide ECS range when assessing future climate impacts.

https://doi.org/10.5194/egusphere-2026-3557
Preprint. Discussion started: 26 June 2026

There are notable regional contrasts between the two basins. While the Atlantic is historically the more active storm track region (Harvey et al., 2020), our projections indicate larger absolute changes in the Pacific in the MMM and most individual models, with the exception of CanESM5. This is noteworthy given that CMIP6 biases (i.e., overestimation of the Atlantic and underestimation of the Pacific) would be expected to inflate projected Atlantic changes relative to the Pacific. That the Pacific nonetheless shows larger projected changes in most models suggests it is intrinsically more sensitive to anthropogenic forcing in this ensemble, a finding consistent with the stronger mid-tropospheric EGR changes identified in the Pacific during DJF.

The results also have direct implications for climate policy. While the spatial patterns of projected storm track changes are broadly similar under both scenarios, their magnitude and geographic extent are substantially greater under SSP5-8.5 than SSP2-4.5. This underlines the importance of emissions mitigation: limiting greenhouse gas concentrations to SSP2-4.5-compatible levels substantially reduces the magnitude of storm track shifts and associated precipitation extremes, particularly the poleward enhancement in DJF. The LE framework is directly relevant to risk assessment, as it provides policymakers with a quantified range of plausible outcomes rather than a single deterministic projection, critical for designing adaptation measures that are robust across the range of internal variability.

The primary limitation of this study is the use of only three models, which constrains the assessment of structural uncertainty relative to larger CMIP6 ensembles. Certain analyses, specifically the EGR mechanism diagnostics and precipitation composites, are presented for MPI only in the main text, with CanESM5 in the Supplementary Information, owing to data availability constraints for EC-Earth3 and the fact that MPI and CanESM5 span the full ECS range of the ensemble. However, the consistency of the large-scale storm track responses across all three models supports the inference that these results are broadly representative. The persistent CMIP6 storm track biases, particularly over the Pacific, introduce additional uncertainty in the absolute magnitude of projected changes, and associated climate risk may not be accurately estimated in all regions as a result. Furthermore, this study does not separate the contributions of greenhouse gas increases and anthropogenic aerosol reductions to the projected storm track changes. Both forcings contribute to future NH warming and temperature gradient changes, and their relative roles may differ between basins and seasons (Undorf et al., 2018; Kang et al., 2024). The differences between SSP2-4.5 and SSP5-8.5 reflect distinct trajectories in both aerosol and GHG emissions simultaneously, and disentangling these contributions would require dedicated single-forcing LE experiments beyond the scope of the present study.

Future work should expand the analysis to additional CMIP6 LE models and, when available, CMIP7 LEs, to better constrain structural uncertainty. Higher-resolution models would better resolve fine-scale storm track dynamics and localised precipitation extremes relevant to regional impact assessment. Investigating connections between storm track changes and related circulation features, including blocking frequency, jet stream variability, and the North Atlantic Oscillation, would further elucidate the mechanisms governing regional precipitation responses. Finally, assessing the socioeconomic impacts of the projected storm track changes and investigating the efficiency of adaptation and risk management approaches would extend the value of this work for policy and decision-making.

https://doi.org/10.5194/egusphere-2026-3557
Preprint. Discussion started: 26 June 2026

Data Availability

All CMIP6 data used in this study are available via the ESGF portal at *https://aims2.llnl.gov/search*. ERA5 reanalysis data are available from the Copernicus Climate Data Store at *https://cds.climate.copernicus.eu*.

Author contribution

KEH and MAB designed the study. KEH performed the analysis and wrote the original draft of the manuscript. KEH and MAB discussed the results and interpreted the findings. BS provided suggestions on the analysis and interpretation of the results, and finalised the manuscript writing.

Competing interests

The authors declare that they have no conflict of interest.

Acknowledgements

The authors thank the modelling groups who contributed to CMIP6 and made their large ensemble simulations available through the MMLEA. ERA5 data were provided by the Copernicus Climate Change Service.

Financial support

We acknowledge support from the UK Natural Environment Research Council (NERC) grant NE/N006038/1.

References

Bell, G. D. and Bosart, L. F.: A 15-Year Climatology of Northern Hemisphere 500 mb Closed Cyclone and Anticyclone Centers, Monthly Weather Review, 117, 2142–2164, https://doi.org/10.1175/1520-0493(1989)117<2142:AYCONH>2.0.CO;2, 1989.

Blackmon, M. L.: A Climatological Spectral Study of the 500 mb Geopotential Height of the Northern Hemisphere, Journal of Atmospheric Sciences, 33, 1607–1623, https://doi.org/10.1175/1520-0469(1976)033<1607:ACSSOT>2.0.CO;2, 1976.

Catto, J. L., Shaffrey, L. C., and Hodges, K. I.: Northern Hemisphere Extratropical Cyclones in a Warming Climate in the HiGEM High-Resolution Climate Model, Journal of Climate, 24, 5336–5352, https://doi.org/10.1175/2011JCLI4181.1, 2011.

Chang, E. K.-M., Yau, A. M.-W., and Zhang, R.: Finding Storm Track Activity Metrics That Are Highly Correlated with Weather Impacts. Part II: Estimating Precipitation Change Associated with Projected Storm Track Change over Europe, Journal of Climate, 35, 2423–2440, https://doi.org/10.1175/JCLI-D-21-0259.1, 2022.

Chang, E. K. M. and Fu, Y.: Interdecadal Variations in Northern Hemisphere Winter Storm Track Intensity, Journal of Climate, 15, 642–658, https://doi.org/10.1175/1520-0442(2002)015<0642:IVINHW>2.0.CO;2, 2002.

Chang, E. K. M. and Yau, A. M. W.: Northern Hemisphere winter storm track trends since 1959 derived from multiple reanalysis datasets, Climate Dynamics, 47, 1435–1454, 10.1007/s00382-015-2911-8, 2016.

Chang, E. K. M., Guo, Y., and Xia, X.: CMIP5 multimodel ensemble projection of storm track change under global warming, Journal of Geophysical Research: Atmospheres, 117, https://doi.org/10.1029/2012JD018578, 2012.

Chang, E. K. M., Ma, C.-G., Zheng, C., and Yau, A. M. W.: Observed and projected decrease in Northern Hemisphere extratropical cyclone activity in summer and its impacts on maximum temperature, Geophysical Research Letters, 43, 2200–2208, https://doi.org/10.1002/2016GL068172, 2016.

https://doi.org/10.5194/egusphere-2026-3557
Preprint. Discussion started: 26 June 2026

Chemke, R. and Coumou, D.: Human influence on the recent weakening of storm tracks in boreal summer, npj Climate and Atmospheric Science, 7, 86, 10.1038/s41612-024-00640-2, 2024.
Coumou, D., Lehmann, J., and Beckmann, J.: The weakening summer circulation in the Northern Hemisphere mid-latitudes, Science, 348, 324–327, 10.1126/science.1261768, 2015.
Deser, C., Lehner, F., Rodgers, K. B., Ault, T., Delworth, T. L., DiNezio, P. N., Fiore, A., Frankignoul, C., Fyfe, J. C., Horton, D. E., Kay, J. E., Knutti, R., Lovenduski, N. S., Marotzke, J., McKinnon, K. A., Minobe, S., Randerson, J., Screen, J. A., Simpson, I. R., and Ting, M.: Insights from Earth system model initial-condition large ensembles and future prospects, Nature Climate Change, 10, 277–286, 10.1038/s41558-020-0731-2, 2020.
Döscher, R., Acosta, M., Alessandri, A., Anthoni, P., Arsouze, T., Bergman, T., Bernardello, R., Boussetta, S., Caron, L. P., Carver, G., Castrillo, M., Catalano, F., Cvijanovic, I., Davini, P., Dekker, E., Doblas-Reyes, F. J., Docquier, D., Echevarria, P., Fladrich, U., Fuentes-Franco, R., Gröger, M., v. Hardenberg, J., Hieronymus, J., Karami, M. P., Keskinen, J. P., Koenigk, T., Makkonen, R., Massonnet, F., Ménégoz, M., Miller, P. A., Moreno-Chamarro, E., Nieradzik, L., van Noije, T., Nolan, P., O'Donnell, D., Ollinaho, P., van den Oord, G., Ortega, P., Prims, O. T., Ramos, A., Reerink, T., Rousset, C., Ruprich-Robert, Y., Le Sager, P., Schmith, T., Schrödner, R., Serva, F., Sicardi, V., Sloth Madsen, M., Smith, B., Tian, T., Tourigny, E., Uotila, P., Vancoppenolle, M., Wang, S., Wårlind, D., Willén, U., Wyser, K., Yang, S., Yepes-Arbós, X., and Zhang, Q.: The EC-Earth3 Earth system model for the Coupled Model Intercomparison Project 6, Geosci. Model Dev., 15, 2973–3020, 10.5194/gmd-15-2973-2022, 2022.
García-Martínez, I. and Bollasina, M. A.: Identifying the evolving human imprint on heat wave trends over the United States and Mexico, Environmental Research Letters, 16, 094039, 10.1088/1748-9326/ac1edb, 2021.
Geng, Q. and Sugi, M.: Variability of the North Atlantic Cyclone Activity in Winter Analyzed from NCEP–NCAR Reanalysis Data, Journal of Climate, 14, 3863–3873, https://doi.org/10.1175/1520-0442(2001)014<3863:VOTNAC>2.0.CO;2, 2001.
Geng, Q. and Sugi, M.: Possible Change of Extratropical Cyclone Activity due to Enhanced Greenhouse Gases and Sulfate Aerosols—Study with a High-Resolution AGCM, Journal of Climate, 16, 2262–2274, https://doi.org/10.1175/1520-0442(2003)16<2262:PCOECA>2.0.CO;2, 2003.
Graham, N. E. and Diaz, H. F.: Evidence for Intensification of North Pacific Winter Cyclones since 1948, Bulletin of the American Meteorological Society, 82, 1869–1894, https://doi.org/10.1175/1520-0477(2001)082<1869:EFIONP>2.3.CO;2, 2001.
Harvey, B. J., Cook, P., Shaffrey, L. C., and Schiemann, R.: The Response of the Northern Hemisphere Storm Tracks and Jet Streams to Climate Change in the CMIP3, CMIP5, and CMIP6 Climate Models, Journal of Geophysical Research: Atmospheres, 125, e2020JD032701, https://doi.org/10.1029/2020JD032701, 2020.
Hausfather, Z. and Peters, G. P.: Emissions – the 'business as usual' story is misleading, Nature, 577, 618–620, 10.1038/d41586-020-00177-3, 2020.
Hawcroft, M., Walsh, E., Hodges, K., and Zappa, G.: Significantly increased extreme precipitation expected in Europe and North America from extratropical cyclones, Environmental Research Letters, 13, 124006, 10.1088/1748-9326/aaed59, 2018.
Hawcroft, M. K., Shaffrey, L. C., Hodges, K. I., and Dacre, H. F.: How much Northern Hemisphere precipitation is associated with extratropical cyclones?, Geophysical Research Letters, 39, https://doi.org/10.1029/2012GL053866, 2012.
Held, I. M.: Large-Scale Dynamics and Global Warming, Bulletin of the American Meteorological Society, 74, 228–242, https://doi.org/10.1175/1520-0477(1993)074<0228:LSDAGW>2.0.CO;2, 1993.
Hersbach, H., Bell, B., Berrisford, P., Hirahara, S., Horányi, A., Muñoz-Sabater, J., Nicolas, J., Peubey, C., Radu, R., Schepers, D., Simmons, A., Soci, C., Abdalla, S., Abellan, X., Balsamo, G., Bechtold, P., Biavati, G., Bidlot, J., Bonavita, M., De Chiara, G., Dahlgren, P., Dee, D., Diamantakis, M., Dragani, R., Flemming, J., Forbes, R., Fuentes, M., Geer, A., Haimberger, L., Healy, S., Hogan, R. J., Hólm, E., Janisková, M., Keeley, S., Laloyaux, P., Lopez, P., Lupu, C., Radnoti, G., de Rosnay, P., Rozum, I., Vamborg, F., Villaume, S., and Thépaut, J.-N.: The ERA5 global reanalysis, Quarterly Journal of the Royal Meteorological Society, 146, 1999–2049, https://doi.org/10.1002/qj.3803, 2020.
Hess, O. and Chemke, R.: Forced Changes in the North Atlantic Storm Track Over the Last Millennium, Geophysical Research Letters, 52, e2025GL115894, https://doi.org/10.1029/2025GL115894, 2025.
Hodges, K. I.: Adaptive constraints for feature tracking, Mon. Wea. Rev., 127, 1362–1373, https://doi.org/10.1175/1520-0493(1999)127<1362:ACFFT>2.0.CO;2, 1999.
Holland, M. M. and Bitz, C. M.: Polar amplification of climate change in coupled models, Climate Dynamics, 21, 221–232, 10.1007/s00382-003-0332-6, 2003.

https://doi.org/10.5194/egusphere-2026-3557
Preprint. Discussion started: 26 June 2026

Hoskins, B. J. and Hodges, K. I.: New Perspectives on the Northern Hemisphere Winter Storm Tracks, Journal of the Atmospheric Sciences, 59, 1041–1061, https://doi.org/10.1175/1520-0469(2002)059<1041:NPOTNH>2.0.CO;2, 2002.

Hoskins, B. J. and Hodges, K. I.: The Annual Cycle of Northern Hemisphere Storm Tracks. Part I: Seasons, Journal of Climate, 32, 1743–1760, https://doi.org/10.1175/JCLI-D-17-0870.1, 2019.

Jucker, M., Pepler, A., Paget, G., and Burke, C.: Global representation of extratropical cyclone precipitation and future trends in CMIP6 models, Quarterly Journal of the Royal Meteorological Society, 151, e5010, https://doi.org/10.1002/qj.5010, 2025.

Kang, J. M., Shaw, T. A., and Sun, L.: Anthropogenic Aerosols Have Significantly Weakened the Regional Summertime Circulation in the Northern Hemisphere During the Satellite Era, AGU Advances, 5, e2024AV001318, https://doi.org/10.1029/2024AV001318, 2024.

Karwat, A., Franzke, C. L. E., and Blender, R.: Long-Term Trends of Northern Hemispheric Winter Cyclones in the Extended ERA5 Reanalysis, Journal of Geophysical Research: Atmospheres, 127, e2022JD036952, https://doi.org/10.1029/2022JD036952, 2022.

Laurila, T. K., Sinclair, V. A., and Gregow, H.: Climatology, variability, and trends in near-surface wind speeds over the North Atlantic and Europe during 1979–2018 based on ERA5, International Journal of Climatology, 41, 2253–2278, https://doi.org/10.1002/joc.6957, 2021.

Lehmann, J., Coumou, D., Frieler, K., Eliseev, A. V., and Levermann, A.: Future changes in extratropical storm tracks and baroclinicity under climate change, Environmental Research Letters, 9, 084002, 10.1088/1748-9326/9/8/084002, 2014.

Lu, J. and Cai, M.: Seasonality of polar surface warming amplification in climate simulations, Geophysical Research Letters, 36, https://doi.org/10.1029/2009GL040133, 2009.

Maher, N., Milinski, S., Suarez-Gutierrez, L., Botzet, M., Dobrynin, M., Kornblueh, L., Kröger, J., Takano, Y., Ghosh, R., Hedemann, C., Li, C., Li, H., Manzini, E., Notz, D., Putrasahan, D., Boysen, L., Claussen, M., Ilyina, T., Olonscheck, D., Raddatz, T., Stevens, B., and Marotzke, J.: The Max Planck Institute Grand Ensemble: Enabling the Exploration of Climate System Variability, Journal of Advances in Modeling Earth Systems, 11, 2050–2069, https://doi.org/10.1029/2019MS001639, 2019.

Mankin, J. S., Lehner, F., Coats, S., and McKinnon, K. A.: The Value of Initial Condition Large Ensembles to Robust Adaptation Decision-Making, Earth's Future, 8, e2012EF001610, https://doi.org/10.1029/2020EF001610, 2020.

McKenna, C. M. and Maycock, A. C.: The Role of the North Atlantic Oscillation for Projections of Winter Mean Precipitation in Europe, Geophysical Research Letters, 49, e2022GL099083, https://doi.org/10.1029/2022GL099083, 2022.

Mercier, L. C., Afargan-Gerstman, H., Priestley, M. D. K., Christensen, J. H., and Domeisen, D. I. V.: Extreme Extratropical Cyclones in a Warmer Climate: Assessing Signal Robustness and Model Uncertainty, EGUsphere, 2026, 1–24, 10.5194/egusphere-2026-1805, 2026.

Murray, R. J. and Simmonds, I.: A numerical scheme for tracking cyclone centres from digital data Part I: development and operation of the scheme, Australian Meteorological Magazine, 39, 155–166, 10.1071/ES91020, 1991.

Olonscheck, D., Suarez-Gutierrez, L., Milinski, S., Beobide-Arsuaga, G., Baehr, J., Fröb, F., Ilyina, T., Kadow, C., Krieger, D., Li, H., Marotzke, J., Plésiat, É., Schupfner, M., Wachsmann, F., Wallberg, L., Wieners, K.-H., and Brune, S.: The New Max Planck Institute Grand Ensemble With CMIP6 Forcing and High-Frequency Model Output, Journal of Advances in Modeling Earth Systems, 15, e2023MS003790, https://doi.org/10.1029/2023MS003790, 2023.

Park, M. and Lee, S.: A Mechanism for the Midwinter Minimum in North Pacific Storm-Track Intensity From a Global Perspective, Geophysical Research Letters, 47, e2019GL086052, https://doi.org/10.1029/2019GL086052, 2020.

Pfahl, S. and Wernli, H.: Quantifying the Relevance of Cyclones for Precipitation Extremes, Journal of Climate, 25, 6770–6780, https://doi.org/10.1175/JCLI-D-11-00705.1, 2012.

Priestley, M. D. K. and Catto, J. L.: Future changes in the extratropical storm tracks and cyclone intensity, wind speed, and structure, Weather Clim. Dynam., 3, 337–360, 10.5194/wcd-3-337-2022, 2022.

Priestley, M. D. K., Ackerley, D., Catto, J. L., Hodges, K. I., McDonald, R. E., and Lee, R. W.: An Overview of the Extratropical Storm Tracks in CMIP6 Historical Simulations, Journal of Climate, 33, 6315–6343, https://doi.org/10.1175/JCLI-D-19-0928.1, 2020.

Priestley, M. D. K., Stephenson, D. B., Scaife, A. A., Bannister, D., Allen, C. J. T., and Wilkie, D.: Forced trends and internal variability in climate change projections of extreme European windstorm frequency and severity, Quarterly Journal of the Royal Meteorological Society, 150, 4933–4950, https://doi.org/10.1002/qj.4849, 2024.

https://doi.org/10.5194/egusphere-2026-3557
Preprint. Discussion started: 26 June 2026

Rivosecchi, A., Bollasina, M. A., and Colfescu, I.: Future changes in the influence of the NAO on Mediterranean winter precipitation extremes in the EC-Earth3 large Ensemble: The prominent role of internal variability, Atmospheric Research, 304, 107391, https://doi.org/10.1016/j.atmosres.2024.107391, 2024.

Screen, J. A., Audette, A., Blackport, R., Deser, C., England, M., Feldl, N., Gervais, M., Hay, S., Kushner, P. J., Liang, Y.-C., Msadek, R., Mudhar, R., Sigmond, M., Smith, D., Sun, L., and Yu, H.: Causes and consequences of Arctic amplification elucidated by coordinated multimodel experiments, Communications Earth & Environment, 7, 23, 10.1038/s43247-025-03052-z, 2025.

Seneviratne, S. I., Zhang, X., Adnan, M., Badi, W., Dereczynski, C., Di Luca, A., Ghosh, S., Iskandar, I., Kossin, J., Lewis, S., Otto, F., Pinto, I., Satoh, M., Vicente-Serrano, S. M., Wehner, M., and Zhou, B.: Weather and Climate Extreme Events in a Changing Climate, in: Climate Change 2021: The Physical Science Basis. Contribution of Working Group I to the Sixth Assessment Report of the Intergovernmental Panel on Climate Change, edited by: Masson-Delmotte, V., Zhai, P., Pirani, A., Connors, S. L., Péan, C., Berger, S., Caud, N., Chen, Y., Goldfarb, L., Gomis, M. I., Huang, M., Leitzell, K., Lonnoy, E., Matthews, J. B. R., Maycock, T. K., Waterfield, T., Yelekçi, O., Yu, R., and Zhou, B., Cambridge University Press, Cambridge, United Kingdom and New York, NY, USA, 1513–1766, 10.1017/9781009157896.013, 2021.

Shaw, T. A., Arblaster, J. M., Birner, T., Butler, A. H., Domeisen, D. I. V., Garfinkel, C. I., Garny, H., Grise, K. M., and Karpechko, A. Y.: Emerging Climate Change Signals in Atmospheric Circulation, AGU Advances, 5, e2024AV001297, https://doi.org/10.1029/2024AV001297, 2024.

Shaw, T. A., Baldwin, M., Barnes, E. A., Caballero, R., Garfinkel, C. I., Hwang, Y. T., Li, C., O'Gorman, P. A., Rivière, G., Simpson, I. R., and Voigt, A.: Storm track processes and the opposing influences of climate change, Nature Geoscience, 9, 656–664, 10.1038/ngeo2783, 2016.

Simpson, I. R., Shaw, T. A., Ceppi, P., Clement, A. C., Fischer, E., Grise, K. M., Pendergrass, A. G., Screen, J. A., Wills, R. C. J., Woollings, T., Blackport, R., Kang, J. M., and Po-Chedley, S.: Confronting Earth System Model trends with observations, Science Advances, 11, eadt8035, 10.1126/sciadv.adt8035, 2025.

Swart, N. C., Cole, J. N. S., Kharin, V. V., Lazare, M., Scinocca, J. F., Gillett, N. P., Anstey, J., Arora, V., Christian, J. R., Hanna, S., Jiao, Y., Lee, W. G., Majaess, F., Saenko, O. A., Seiler, C., Seinen, C., Shao, A., Sigmond, M., Solheim, L., von Salzen, K., Yang, D., and Winter, B.: The Canadian Earth System Model version 5 (CanESM5.0.3), Geosci. Model Dev., 12, 4823–4873, 10.5194/gmd-12-4823-2019, 2019.

Undorf, S., Bollasina, M. A., and Hegerl, G. C.: Impacts of the 1900–74 Increase in Anthropogenic Aerosol Emissions from North America and Europe on Eurasian Summer Climate, Journal of Climate, 31, 8381–8399, https://doi.org/10.1175/JCLI-D-17-0850.1, 2018.

Virgin, J. G., Fletcher, C. G., Cole, J. N. S., von Salzen, K., and Mitovski, T.: Cloud Feedbacks from CanESM2 to CanESM5.0 and their influence on climate sensitivity, Geosci. Model Dev., 14, 5355–5372, 10.5194/gmd-14-5355-2021, 2021.

Wallace, J. M., Lim, G.-H., and Blackmon, M. L.: Relationship between Cyclone Tracks, Anticyclone Tracks and Baroclinic Waveguides, Journal of Atmospheric Sciences, 45, 439–462, https://doi.org/10.1175/1520-0469(1988)045<0439:RBCTAT>2.0.CO;2, 1988.

Wyser, K., van Noije, T., Yang, S., von Hardenberg, J., O'Donnell, D., and Döscher, R.: On the increased climate sensitivity in the EC-Earth model from CMIP5 to CMIP6, Geosci. Model Dev., 13, 3465–3474, 10.5194/gmd-13-3465-2020, 2020.

Yau, A. M.-W. and Chang, E. K.-M.: Finding Storm Track Activity Metrics That Are Highly Correlated with Weather Impacts. Part I: Frameworks for Evaluation and Accumulated Track Activity, Journal of Climate, 33, 10169–10186, https://doi.org/10.1175/JCLI-D-20-0393.1, 2020.

Yin, J. H.: A consistent poleward shift of the storm tracks in simulations of 21st century climate, Geophysical Research Letters, 32, https://doi.org/10.1029/2005GL023684, 2005.